CaV1.3-driven SK channel activation regulates pacemaking and spike frequency adaptation in mouse chromaffin cells

David H. F. Vandael, Annalisa Zuccotti, Joerg Striessnig, Emilio Carbone
CaV1.3-driven SK channel activation regulates pacemaking and spike frequency adaptation in mouse chromaffin cells
THE JOURNAL OF NEUROSCIENCE (2012) 32
DOI: 10.1523/JNEUROSCI.3715-12.2012

The Journal of Neuroscience

http://jneurosci.msubmit.net

CaV1.3-driven SK channel activation regulates pacemaking and spike frequency adaptation in mouse chromaffin cells

JN-RM-3715-12R1

Emilio Carbone, University of Turin

David Vandael, Heinrich-Heine-University

Annalisa Zuccotti, University of Tübingen

Jörg Striessnig, University of Innsbruck

Commercial Interest: No

$Ca_V1.3$-driven SK channel activation regulates pacemaking and spike frequency adaptation in mouse chromaffin cells

David H.F. Vandael[1], Annalisa Zuccotti[2¤], Joerg Striessnig[3], Emilio Carbone[1§]

[1]*Department of Drug Science, Laboratory of Cellular and Molecular Neuroscience, NIS Center, 10125 Torino, Italy*
[2]*Department of Otolaryngology, University of Tübingen, 72076 Tübingen, Germany*
[3]*Institute of Pharmacy, Pharmacology and Toxicology, A-6020 Innsbruck, Austria*

Abbreviated title: $Ca_V1.3$-activated SK currents regulate phasic firing in chromaffin cells

§ *Corresponding author:* Emilio Carbone
Department of Drug Science
Corso Raffaello 30
10125 - Torino, Italy

tel.: +39.011.670.8489
fax: +39.011.670.8174
e-mail: emilio.carbone@unito.it

Number of pages: 32
Number of figures: 9
Number of words: Abstract 243, Introduction 509, Discussion 1561

Acknowledgments: We thank Dr. C. Franchino for preparing the cell cultures and Prof. V. Carabelli and Dr. A. Marcantoni for helpful discussions. We also thank Prof. J. Engel (Homburg) for supplying $Ca_V1.3^{-/-}$ breeding pairs. This work was supported by the Marie Curie Research Training Network "CavNET" (Contract No MRTN-CT-2006-035367), the Regione Piemonte POR/FERS program (grant # 186-111C), the Unito-San Paolo Company research grant 2011-2013 and the Austrian Science Fund (P20670).

The authors declare no competing financial interests

¤ *Present address:* Department of Clinical Neurobiology, German Cancer Research Center (DKFZ), Heidelberg University Medical Center, 69120 Heidelberg (Germany)

Abstract

Mouse chromaffin cells (MCCs) fire spontaneous action potentials (APs) at rest. $Ca_v1.3$ L-type calcium channels (LTCCs) sustain the pacemaker current and their loss results in depolarized resting potentials (V_{rest}), spike broadening and remarkable switches into depolarization block after BayK 8644 application. A functional coupling between $Ca_v1.3$ and BK channels has been reported but cannot fully account for the aforementioned observations.

Here, using $Ca_v1.3^{-/-}$ mice, we investigated the role of $Ca_v1.3$ on SK channel activation and how this functional coupling affects the firing patterns induced by sustained current injections. MCCs express SK1-3 channels, whose tonic currents are responsible for the slow irregular firing observed at rest. Percentage of frequency-increase induced by apamin was found inversely correlated to basal firing frequency. Upon stimulation, MCCs build-up $Ca_v1.3$-dependent SK currents during the interspike intervals that lead to a notable degree of spike frequency adaptation (SFA). The major contribution of $Ca_v1.3$ to the sub-threshold Ca^{2+}-charge during an AP-train rather than a specific molecular coupling to SK channels accounts for the reduced SFA of $Ca_v1.3^{-/-}$ MCCs. Low adaptation ratios due to reduced SK activation associated with $Ca_v1.3$ deficiency prevent the efficient recovery of Na_V channels from inactivation. This promotes a rapid decline of AP amplitudes and facilitates early onset of depolarization-block following prolonged stimulation. Thus, besides serving as pacemaker, $Ca_v1.3$ slows-down MCC firing by activating SK channels that maintain Na_V channel availability high enough to preserve stable AP waveforms, even upon high-frequency stimulation of chromaffin cells during stress responses.

Introduction

Mouse chromaffin cells (MCCs) are neuroendocrine cells endowed with a diverse set of ion conductances that permit the spontaneous generation and efficient termination of action potentials (APs). L-type calcium channels (LTCCs) have been shown to fulfill the role of pacemaker channels in MCCs (Marcantoni et al. 2010). $Ca_v1.3$ LTCCs in particular were shown to contribute to the pacemaker current passing during the interspike intervals (ISIs) due to their low-threshold of activation, fast activation kinetics and slower inactivation of I_{Ca} (Vandael et al. 2010). Loss of $Ca_v1.3$ resulted in a reduction of the fraction of spontaneously firing MCCs, and led to a depolarized resting potential (V_m) (Mahapatra et al. 2011). $Ca_v1.3^{-/-}$ MCCs that remained spontaneously active, fired at higher frequencies as compared to wild-type (WT) MCCs and responded to the LTCC activator BayK 8644 with a strong sustained membrane depolarization. An aberrant activation of BK channels contributes but does not fully account for this phenomenon, suggesting a possible contribution of other Ca^{2+}-activated K^+ channels, such as SK channels (Vandael et al., 2010).

SK channels are widely expressed throughout the central and peripheral nervous system where they act as crucial modulators of cellular excitability (Stocker, 2004; Faber, 2009). Besides affecting firing frequencies, SK channels are involved in switches from single spiking- into burst-firing patterns and can drive spike frequency adaptation (SFA) and accommodation (Engel et al., 1999; Wolfart et al., 2001; Hallworth et al., 2003). SK currents contribute to the afterhyperpolarization (AHP) phase of single or bursts of APs, slowing-down the pacemaker cycle. SK channel's high Ca^{2+}-sensitivity lays at the basis of the prevailing current view that SK channels do not have to be necessarily close to a specific Ca^{2+} source to get activated (Fakler and Adelman, 2008). Several studies nevertheless demonstrated a specific coupling of SK channels to voltage gated calcium channels (VGCCs) or neurotransmitter receptors (Marion and Tavalin, 2000; Oliver et al., 2000; Shah and Haylett, 2002; Cueni et al., 2008; Engbers et al., 2012).

In chromaffin cells, SK channels were first biophysically identified in bovine (BCCs) and in rat chromaffin cells (RCCs) (Marty and Neher, 1985; Neely and Lingle, 1992). Experiments performed on cat adrenals revealed that secretion of catecholamines induced by electrical stimulation or acetylcholine application could be potently stimulated by SK block (Montiel et al., 1995). Up to now, however, nothing is known about the role of SK channels on MCCs excitability and how SK channels relate to L- and non-LTCCs. Here we give evidence for a key role of $Ca_v1.3$ LTCCs in triggering the activation of sub-threshold SK currents that introduce a strong degree of SFA in MCCs. $Ca_v1.3$ deficiency results in elevated degrees of Na^+ channel inactivation upon current injections that impedes the maintenance of sustained physiological firing patterns.

This dual role of $Ca_v1.3$ to serve as “drive” and “brake” to phasically adapt AP firing of MCCs may be determinant for limiting catecholamine release during sustained stress stimuli and might be at the basis of SFA of several central neurons characterized by slow frequency AP firing driven by LTCCs (see Vandael et al., 2010).

Materials and methods

Wild-type and $Ca_v1.3^{-/-}$ mouse chromaffin cell culture

Chromaffin cells were obtained from male C57BL/6N mice of 3 months (Harlan, Correzzano, Italy). Like in our previous works (Marcantoni et al., 2010; Mahapatra et al., 2011), $Ca_v1.3^{-/-}$ mice (Platzer et al., 2000) were obtained from the animal house of the Eberhard Karls Universität Tübingen (Germany) bred under SPF conditions locally. All experiments were conducted in accordance with the National Guide for the Care and Use of Laboratory Animals adopted by the Italian Ministry of Health. For removal of tissues, animals were sacrificed by cervical dislocation. Culture procedure was adapted from Marcantoni et al. (2010) with slight modifications. Under sterile conditions the abdomen was opened, the adrenal glands were isolated, and transfered to an ice cold Ca^{2+} and Mg^{2+} free Locke’s buffer containing (in mM) 154 NaCl, 3.6 KCl, 5.6 $NaHCO_3$, 5.6 glucose and 10 HEPES, pH 7.4. Under a dissecting microscope the adrenal glands were decapsulated and subsequently subjected to an enzymatic dissociation with 20-25 Units/ml papain (Worthington Biochemical Corp., Lakewood, NJ, USA) dissolved in DMEM (Life Technologies Italia, Monza, Italy) supplemented with 1.5 mM L-cysteine, 1 mM $CaCl_2$ and 0.5 mM EDTA (Sigma Aldrich, Munich, Germany) for 25 -30 minutes at 37°C in a water saturated atmosphere with 5% CO_2. Subsequently, two washing steps were performed with DMEM supplemented with 1 mM $CaCl_2$ and 10 mg/ml BSA (Sigma Aldrich). Adrenal medulla's were resuspended in DMEM containing 1% pen/strep and 15% fetal bovine serum (FBS) (Sigma Aldrich) and were mechanically dissociated with a fire polished pasteur pipette. A drop (100 µl) of this concentrated cell suspension was plated on poly-ornitine (1 mg/ml) and laminin (5 µg/ml) (Sigma Aldrich) coated petri-dishes and subsequently (30 minutes later) 1.9 ml DMEM containing 1% pen/strep and 15% FBS was added. The primary chromaffin cell culture was kept in an incubator at 37°C at water saturated atmosphere with 5% CO_2.

Electrophysiology

Currents and APs were recorded in perforated-patch conditions using a Multiclamp 700B microelectrode amplifier and pClamp 10.0 software (Molecular Devices, Sunnyvale, CA, USA). Traces were sampled at 10

kHz using a digidata 1440A acquisition interface (Molecular Devices) and filtered using a low-pass Bessel filter set at 1-2 kHz. Borosillicate glass pipettes (Kimble Chase, Vineland, NJ, USA) with a resistance of 2-3 MΩ were dipped in an Eppendorf tube containing an intracellular solution with different composition according to the experimental aim (see below) and then back-filled with the same solution containing 500 µg/ml of amphotericin B dissolved in DMSO (Sigma Aldrich). Recordings were initiated after amphotericin B lowered the access resistance below 15 MΩ (5-10 min). Series resistance was compensated by 80% and monitored throughout the experiment. Fast capacitive transients during step-wise voltage-clamp depolarisations were minimized online using the patch-clamp analogue compensation. Uncompensated capacitive currents were further reduced by subtracting the averaged currents in response to P/4 hyperpolarising pulses. Holding potential (V_h) in voltage-clamp mode was set at -70 mV except when we used dihydropyridines (DHPs). Given that V_{rest} approximates -50 mV and given the voltage-dependency of DHP binding (Mahapatra et al., 2011), V_h was set at -50 mV in voltage-clamp experiments when the LTCC contribution to the total Ca^{2+} current and the Ca^{2+} channel selectivity of SK channel activation was tested by means of selective Ca^{2+} channel blockers (nifedipine and ω-toxins; see below). When we switched to the current-clamp mode, the input cell resistance was measured by injecting a hyperpolarizing current of -10 pA, starting from V_h= -70 mV. Normal current-clamp mode was performed without any correction of the slow patch-clamp response to fast current injections since results have been shown to be similar as those obtained in fast current-clamp mode as described in Marcantoni et al. (2010). The AP-clamp experiments undertaken to reveal the SK current were performed by stimulating each single cell in current-clamp mode with 15 pA current injection, starting from a V_h of -80 to -70 mV, using the cell's own APs as voltage-clamp command. When measuring Ca^{2+} currents flowing during the AP waveform, CsCl was present in the intracellular solution to block K^+ (and Na^+) currents and no APs could be evoked. In this case we used representative AP-trains as voltage-clamp stimulus.

Solutions

For current-, AP- and voltage-clamp recordings of K^+ and Na^+ currents the intracellular solution contained (in mM) 135 KAsp, 8 NaCl, 20 HEPES, 2 $MgCl_2$, 5 EGTA, pH 7.4 (with NaOH; Sigma Aldrich). For Ca^{2+} current recordings the intracellular solution contained (in mM) 135 Cs-MeSO3, 8 NaCl, 2 $MgCl_2$ and 20 HEPES, pH 7,4 (with CsOH; Sigma Aldrich). For current-clamp and K^+ current recordings in voltage- and AP-clamp the extracellular solution was a physiological Tyrode containing (in mM): 30 NaCl, 4 KCl, 2 $CaCl_2$, 2 $MgCl_2$, 10 HEPES and 10 glucose; pH 7.4 (with NaOH; Sigma Aldrich). SK currents were measured in the voltage-

clamp mode using a Tyrode's solution with varying K^+ concentrations (2, 4, 6 and 12 mM) depending on the experimental goal. Changes in KCl concentrations were compensated with an identical concentration of NaCl. The extracellular solution used for Ca^{2+} current measurements in voltage- and AP-clamp configuration contained (in mM): 135 TEA, 2 $CaCl_2$, 2 $MgCl_2$, 10 HEPES, 10 glucose, pH 7.4 (with TEA-OH; Sigma Aldrich). For Na^+ current measurements the extracellular solution contained (in mM) 104 NaCl, 30 TEACl, 4 KCl, 2 $CaCl_2$, 2$MgCl_2$, 10 HEPES and 10 glucose, pH 7.4 (with NaOH; Sigma Aldrich). Tetrodotoxin (TTX) (Tocris Bioscience, Bristol, UK) was applied at 300 nM to block Na^+ currents when we recorded Ca^{2+} and SK currents. As reported previously (Mahapatra et al., 2011), Na^+ currents in MCCs were completely blocked by 300 nM TTX. They were fast inactivating and not persistent. To avoid contamination of BK currents during SK current measurements in voltage- and AP-clamp, 1 µM paxilline (Sigma Aldrich) was added. LTCCs were blocked using 3 µM nifedipine (Sigma Aldrich). P/Q-, N- and R-type channels were blocked by 2 µM ω-Agatoxin IVA, 3,2 µM ω-Conotoxin and 400 nM of SNX-482, respectively (Peptide Institute, Osaka, Japan). Total Ca^{2+} current and Ca^{2+}-activated K^+ currents were blocked by 200 µM Cd^{2+}, while SK channels were blocked by 200 nM apamin (Alomone Labs, Jerusalem, Israel) and potentiated by 1 µM 1-EBIO (Tocris). To check for the degree of coupling of the Ca^{2+} source to SK channels we used the cell permeable Ca^{2+} chelators EGTA-AM (20 µM) or BAPTA-AM (20 µM) (Life Technologies).

All solutions were perfused using a gravity based perfusion system as previously described (Marcantoni et al, 2010). Current-clamp data were not corrected for the liquid junction potential (LJP) (15.4 mV at 22 °C) since the blockers tested were used at concentrations that did not affect the LJP any further (0.1-1000 nM apamin). When using extracellular solutions with different $[K^+]_o$ as compared to the Tyrode's standard described above, the LJP was subjected to minor changes (15.5 mV, 15.3 mV and 15.0 mV for solutions containing 2, 6 and 12 mM K^+, respectively) as compared to the 4 mM K^+ Tyrode's standard. In Fig. 1C, data shown were not corrected for the LJP. The LJP for the Na^+ current measurements using the solutions described above was 16.3 mV.

Analysis and statistics

Data analysis and curve fitting were performed using either Clampfit version 10.0 (Molecular Devices, Sunnyvale, CA, USA) or Origin Pro 6.0 (OriginLab Corp., Northampton, MA, USA). Statistical analysis was performed with SPSS statistics 20 software (IBM Corp., Armonk, NY, USA). Data are given as mean ± SEM for n = number of cells. Statistical significance (*p*) was calculated using either the paired/unpaired 2-tailed

Student's t-test or a one-way ANOVA followed by a Bonferroni post-hoc analysis. Data were considered statistically significant with $p \leq 0.05$.

RNA isolation, cDNA synthesis and RT-PCR

For RT-PCR analysis, adrenal medullae were dissected with small forceps and immediately frozen in liquid nitrogen and stored at -80°C before use. RNA was isolated using the RNeasy mini kit (QIAGEN, Hilden, Germany) following the manufacturer's instructions. After reverse transcription using Sensiscript RT kit (QIAGEN, Hilden, Germany), PCR was performed with ready-to-go beads (GE, Healthcare, Freiburg, Germany). The following primers were used: SK1 for 5'-GGACAATGGTGCCGACGACT-3', rev 5'-GTGCAGCCTGCTCCCATGAT-3' (expected size 564 bp); SK2 for 5'-TTCTAACAACCTGGCGCTCT-3', rev 5'-AACTGTATTTCCCTGGCGTG-3' (expected size 354 bp); SK3 for 5'-CTGTCTTGAGAGTAGCCCCG-3', rev 5'-AGCAGCCTTCCTTTTGTGAA-3' (expected size 590 bp); BK1 for 5'-CACATTGTGTTTGTGGGCTC-3', rev 5'-GATGATGGGAATGTTGACCC-3' (expected size 381 bp).

Results

MCCs express KCNN channels which generate "slow tail" currents sensitive to apamin during Ca^{2+} loading

RT-PCR gave evidence of the expression of SK1, SK2 and SK3 mRNA in the medulla isolated from mouse adrenal glands as well as in brain (which served as positive control) (Fig.1A). All bands corresponded to the expected sizes predicted from KCNN1-3 genes. The identity of the bands with SK channel sequence was confirmed by sequencing of PCR products. This clearly indicates that MCCs express all three SK channels besides BK channels (Fig. 1A) that were a matter of interest in previous studies (Marcantoni et al, 2010; Vandael et al., 2010).

SK currents in primary chromaffin cell cultures exhibit typical "slow tails" following Ca^{2+} loading steps which last seconds and faithfully represent K^+ channel deactivation (Neely and Lingle, 1992; Park, 1994; Park et al., 1996). Upon repolarization to negative potentials (from -50 to -120 mV), only voltage-independent channels remain open for prolonged time spans and tail amplitudes measured 30 ms after repolarization onset are free of fast tails of voltage-dependent K^+ channels (Neely and Lingle, 1992; Solaro and Lingle, 1992; Park, 1994). Also the slowly deactivating T-type Ca^{2+} channels are closed after few milliseconds at very negative potentials (Novara et al., 2004; Carabelli et al., 2007). SK tail currents were measured after Ca^{2+} loading steps at 0 mV, where Ca^{2+} channel activation is maximal in 2 mM extracellular Ca^{2+} (Marcantoni et al., 2010).

Loading step duration was set at 250 ms since saturation of the slow tail amplitude occurred at this time (not shown). As illustrated in Fig. 1B, varying the extracellular K^+ concentration from 2 to 6 mM clearly indicates that the measured currents are consistent with a K^+-selective conductance. After correction for the LJP (see Materials and Methods) the currents reverted at Nernst potentials of -110.5, -92.5 and -78.3 mV for 2, 4 and 6 mM extracellular K^+ respectively (Fig. 1B), in good agreement with the predicted reversal potentials of -106 mV (2 mM), -88 mV (4 mM) and -78 mV (6 mM). This also excludes the possibility of a partial contribution of Ca^{2+}-activated Cl^- currents to slow tail currents as reported elsewhere (Korn and Weight, 1987).

Since apamin block is the fingerprint of SK channels we subsequently tested for the apamin sensitivity of slow tail currents. The percentage block of K^+ tail currents by apamin is shown in Fig. 1C and represents pooled outcomes of 24 cells (Fig. 1C). Maximal block was obtained at 1 µM apamin (82.8%) and the dose-response curve was best fitted by a double-sigmoid function with IC_{50} values of 0.3 nM (80% block) and 80 nM (20% block). This might be explained by a co-expression of diverse SK channel α-subunits with different apamin sensitivities (Weatherall et al., 2011). Fig. 1D shows the block of slow tails by 200 nM apamin (red trace) and the current increase induced by the SK enhancer 1-EBIO (1 µM; grey trace). Intracellular solution and extracellular solution contained 4 and 12 mM K^+ respectively, tail currents were measured at -95 mV. The mean peak amplitude at control decreased by ~80% with apamin ($p< 0.001$; n= 39) and nearly doubled with 1-EBIO ($p< 0.001$; n= 6). The incomplete block by apamin (15-20%) might be due to the presence of less apamin-sensitive SK1 channels. The presence of heteromeric SK channels cannot be excluded.

SK channels slow down MCCs spontaneous firing and set the interspike interval

MCCs fire spontaneously under control conditions (Marcantoni et al., 2009; 2010). Application of 200 nM apamin to a spontaneously firing MCC induced a strong and significant increase in the firing rate from 0.7 ± 0.12 Hz up to 2.4 ± 0.2 Hz (n= 14; $p< 0.001$) (Fig. 2A left, B). In addition, we observed that slow firing cells were more sensitive to apamin than fast firing cells, which responded weakly to the SK blocker (Fig. 2B). Given this, we plotted the basal firing frequency against the percentage of frequency increase by apamin and found a remarkable linear relationship between the two parameters (R= -0.85; $p< 0.001$; n= 12) (Fig. 2B). This is strong evidence that slow firing cells are controlled by robust, tonic SK currents that are crucial to set the spontaneous firing of resting MCCs.

Although it has been reported that SK channels enhance precision of firing in globus pallidus- and GABAergic substantia nigra pars reticularis (SNr)- neurons (Deister et al., 2009; Atherton and Bevan, 2005),

in MCCs the opposite seems to be true (Fig. 2A left). The firing pattern of MCCs is slow and rather irregular at control and becomes faster and more regular with apamin. This is convincingly proved by comparing the distribution of the ISI duration in control vs. apamin (Fig. 2C). The mean ISI duration was larger and more broadly distributed at control conditions (grey bars) with respect to apamin (red bars). Taking the coefficient of variation of the two distributions (CV = standard deviation/mean) as an estimate of the regularity of the firing pattern (Fig. 2C inset), we found that after SK block (0.5 ± 0.05) CV was significantly smaller with respect to control (0.9 ± 0.08; $p< 0.001$; n= 13). When basal firing frequencies (mild apamin effects) were plotted against CV we found a negative linear correlation (R= -0.78; p= 0.001; n= 12) (data not shown). This suggests that SK channels are responsible for the slow and irregular firing patterns observed at rest and that upon stimulation they could induce some degree of SFA.

Next we analyzed the effect of blocking SK channels on AP waveforms. The right part of Fig. 2A shows the overlap of the averaged APs in control (black grids in panel A) and in the presence of 200 nM apamin (red grids in panel A). It should be noticed that the increase in MCC excitability was accompanied by a significant depolarization of V_{rest} (from -46.0 ± 1.1 mV to -44.2 ± 1.6 mV; $p< 0.001$; n= 14), consistent with a block of a K^+ conductance (Fig. 2A left). The amplitude of the AHP was -52.4 ± 0.8 mV in control conditions and decreased to -48.5 ± 0.9 mV with apamin ($p< 0.001$; n= 14) (Fig. 2A right). Since Ca^{2+}-activated K^+ channels assist the re-polarization, fastening the return to baseline and beyond, we measured the effects of apamin on the AP half-width. Half-width after perfusion with apamin was 4.2 ± 0.4 ms, which was significantly bigger than the control value 2.8 ± 0.2 ms ($p< 0.001$; n= 14) (Fig. 2A right). Apamin furthermore significantly reduced the AP-overshoot by about a factor 2 (from 26.3 ± 1.7 mV to 13.6 ± 1.5 mV; $p< 0.001$; n= 14) (Fig. 2A). By blocking an effective repolarization one would expect an increase rather than a decrease of the AP-overshoot. Thus, the increased firing frequency in combination with the V_{rest} depolarization and spike broadening induced by apamin likely reduces the recovery of voltage-gated Na^+ (Na_v) channels.

SK channels preserve the high rate of Na_v channel recovery at rest

A reduced availability of transient Na_v channels supporting the spike upstroke is generally reflected in a depolarization of the spike threshold (V_{thresh}) and a gradual decay of dV/dt_{max} (Gettes and Reuter, 1974; Colbert et al., 1997; Mercer et al., 2007; Deister et al., 2009). This information can be easily obtained by displaying the membrane voltage (V) against its first time derivative (dV/dt) resulting in a “phase plane” plot (Jenerick, 1963) for control (black) and apamin (red) (Fig. 2D). V_{thresh} was taken as the point where dV/dt reaches 4% of its maximal value (Khaliq and Bean, 2010) and is indicated by the dashed line in Fig. 2D.

Phase plane plots under control conditions (black traces) were calculated from the APs indicated by the black grids in Fig. 2A. Red phase plane plots at the bottom of panel C were obtained from APs recorded during apamin application, from the onset of the effect up to the level where the action of the drug stabilized. To measure V_{thresh} we used a phase plane plot from the averaged APs in control and after apamin effect was stable. V_{thresh} at control was significantly lower than that with apamin: -27.6 ± 0.5 mV vs. -25.9 ± 0.5 mV ($p< 0.001$, n= 13) (Fig. 2D). dV/dt_{max} was furthermore nearly constant around 60 V/s at control (n = 13) (black squares, Fig. 2E) while it decreased steeply after perfusion with apamin (23.5 ± 4.6 V/s at 9th AP, $p< 0.001$; n = 13) (red dots, Fig. 2E). Both findings thus indicate that less Na_V channels were available during the fast firing patterns induced by apamin.

An important question is thus how Na^+ currents adapt in spontaneously firing MCCs when SK channels are blocked by apamin. To clarify this, we performed AP-clamp experiments using a train of APs in control (left, black) and during apamin exposure (right, red) as a voltage command (Fig. 3A). AP-trains were derived from current-clamp recordings performed before on the same cell (e.g. Fig. 2A). Ca^{2+} and K^+ currents were blocked by 50 µM Cd^{2+} and 30 mM TEA, respectively. Under these conditions, 300 nM TTX (grey trace) fully abolished the control inward currents (black traces), indicating that these currents were carried by TTX-sensitive Na^+ channels (Fig. 3B). The corresponding TTX-sensitive Na^+ currents, obtained by subtracting the trace with TTX from control are shown in Fig. 3C (blue traces). Insets in Fig. 3B show the TTX-sensitive Na^+ current flowing during the 3rd AP (arrows) in control (left) and with apamin (right).

The evolution of the peak Na^+ current amplitude for each spike at control and with apamin is given in the inset of Fig. 3C. In brief, Na^+ currents for all spikes of the AP-train in control conditions had comparable amplitudes ($p> 0.05$; n= 9) while fast AP firing associated with apamin went along with a steep and almost 3-fold decline of Na^+ current peaks ($p< 0.05$; n= 9; Fig. 3C inset). Note that Na^+ influx is limited to the rising phase of the APs and inactivates completely during the falling phase (Fig. 3B insets). Na^+ current amplitude for spike 5 was significantly bigger during control as compared to apamin ($p< 0.05$). Thus, we conclude that the wider APs and the faster firing patterns induced by depolarized V_{rest} evoke a marked Na^+ channel inactivation in MCCs that leads to gradually decreasing AP amplitudes. In other words, apamin decreases Na^+ channel availability during trains of APs by preventing the high rate of Na^+ channel recovery which occurs during normal interspike intervals.

Ca_v1.3 channels are crucial for SK-dependent spike frequency adaptation in MCCs

We have previously shown that loss of Cav1.3 leads to a strong reduction of the percentage of spontaneously active cells (Marcantoni et al., 2010), and that spontaneously active Cav1.3$^{-/-}$ MCCs possess unusually high firing frequencies at elevated V_{rest} values, possibly due to a lower availability of SK channels (as shown in Fig. 2B). Furthermore, nifedipine (3 µM) leads to a marked depolarization of V_{rest}, indicative of a close interaction between LTCCs and Ca^{2+}-activated K^+ channels (Marcantoni et al., 2010). In addition to this, in several central neurons SK channels are shown to be involved in SFA, a process that can be defined as the gradual decrease of the instantaneous firing frequency upon sustained current injections (Benda and Herz, 2003). Thus, we studied whether SK currents lead to SFA in MCCs and whether an aberrant activation of SK currents in the absence of $Ca_v1.3$ LTCCs might interfere with this process. This would explain the previously observed findings reported by Marcantoni et al. (2010).

WT MCCs typically responded to current injections with a train of APs that were marked by a gradual decay of the instantaneous firing frequency. The instantaneous firing frequency toward the end of the pulse (f_{ss}) was always smaller as compared to that measured at onset (f_o), giving rise to an adaptation ratio f_o/f_{ss} always >1 (Fig. 4A). When the current step was increased from 5 to 15 pA, WT MCCs responded with a 2-fold increase of f_o ($p< 0.001$; n= 56) while f_{ss} increased by 1.6-fold, indicative of the adapting behavior of these cells (Fig. 4B left). On the contrary, deletion of Cav1.3 resulted in MCCs that required current steps greater than 5 pA in order to evoke APs (70.6 % of cases). In addition, 15 pA of current led to a significant 1.9-fold increase of f_{ss} in Cav1.3$^{-/-}$ MCCs ($p< 0.001$; n= 28) as compared to WTs (Fig. 4B left). f_o was nearly unaffected, meaning that the adaptation ratio of Cav1.3$^{-/-}$ MCCs is 2-fold lower (2.5 vs 5.1) as compared to WT MCCs for 15 pA current injection.

As expected, apamin (200 nM) lead to elevated firing frequencies in WT MCCs (Fig. 4A bottom). SK block specifically affected f_{ss}, leaving f_o nearly unchanged (Fig. 4B right). For 15 pA current injection, apamin gave rise to a significant 2.2-fold increase of f_{ss} in WT MCCs ($p< 0.001$; n= 23) that strikingly coincides with the value of Cav1.3$^{-/-}$ MCCs in control conditions (Fig. 4B right). Moreover, apamin did not increase f_{ss} of Cav1.3$^{-/-}$ MCCs any further.

Besides monitoring the degree of SFA, we also measured the time course of the adaptation process (Fig. 4C, D). The time constant of the frequency decline (τ_{SFA}) was derived from single exponential fits of the data shown in Fig. 4C and D, which represent the evolution of the instantaneous firing frequency with each ISI. Significant differences ($p< 0.05$) in τ_{SFA} between WT and $Ca_v1.3^{-/-}$ MCCs were only found for 15 pA current

injections (0.9 ± 0.1 and 1.7 ± 0.4, respectively) (Fig. 4C). This clearly indicates that, particularly for higher current steps, adaptation of the firing frequency takes considerably more time in $Ca_v1.3^{-/-}$ MCCs as compared to WT's. Again we found a striking similarity between τ_{SFA} of $Ca_v1.3^{-/-}$ MCCs and WT MCCs perfused with apamin (τ_{SFA} = 2.0 ± 0.7) (Fig. 4D). Notice also that apamin does not affect the development of SFA in $Ca_v1.3^{-/-}$ MCCs any further (Fig. 4D right). It thus results that SFA in $Ca_v1.3^{-/-}$ MCCs is reduced and requires more time to develop than in WT MCCs.

SK block or lack of $Ca_v1.3$ lower the ability to generate sustained AP trains during strong depolarization

The increase of an SK channel conductance that follows gradual intracellular Ca^{2+} accumulation during a train of APs is found to lower the cell resistance (Engel et al., 1999). This in turn contributes to the sequential widening of the ISI duration (slows down the pacemaker cycle) and could furthermore lead to an increase of the input current that the cell can deal with. Since we found that $Ca_v1.3^{-/-}$ MCCs show less SK-dependent SFA, it could be that these cells show an earlier transition into depolarization block (defined as a short train of spikes followed by a sustained membrane depolarization). This hypothesis was tested by looking at the responses of WT and $Ca_v1.3^{-/-}$ MCCs to current injections ranging from 1 to 30 pA (Fig. 5A). We observed that while driving up the current intensity, the adaptation ratio (f_o/f_{ss}) for WT MCCs increased following an exponential function that showed no saturation in the current range tested (τ = 11.7 ± 0.7 pA; R^2 = 0.94; n= 67). $Ca_v1.3^{-/-}$ MCCs (n= 51) as well as WT MCCs perfused with apamin (200 nM) (n = 42) were both characterized by a much faster time constant (τ = 1.6 ± 0.1 pA; R^2= 0.9 and 1.7 ± 0.5 pA; R^2 = 0.9, respectively) as compared to WT MCCs in control conditions (p< 0.001; Fig. 5B).

Panel C illustrates the distributions of the rheobase (minimal amount of current to trigger a spike) for WT and $Ca_v1.3^{-/-}$ MCCs (black and blue, respectively). Mean value of the current required to trigger an AP was 4.0 ± 0.2 pA (n= 56) for WT MCCs and resulted significantly larger (6.6 ± 0.4 pA; p< 0.001; n= 51) for $Ca_v1.3^{-/-}$'s (Fig. 5C). This is not surprising given that $Ca_v1.3$ LTCCs open at rather negative V_m, show weak voltage-dependent inactivation and are characterized by fast activation kinetics (Koschak et al., 2001; Xu and Lipscombe, 2001; Mangoni et al., 2003; Marcantoni et al., 2010). Interestingly we found that the stagnating adaptation ratio of $Ca_v1.3^{-/-}$ MCCs and apamin-treated WT MCCs were correlated with an earlier onset of depolarization block (Fig. 5A bottom). For WT MCCs under control conditions the onset of depolarization block (19.5 ± 0.7 pA; n= 67) was 4.9 and 5.9 pA higher than in apamin-treated WT cells (14.6 ± 0.5 pA; p<

0.001; n= 42) (Fig. 5D) and $Ca_v1.3^{-/-}$ MCCs (13.6 ± 0.6 pA; p< 0.001; n= 51), respectively (Fig. 5E). Thus, loss of $Ca_v1.3$ LTCCs or block of SK channels, reduces the ability of MCCs to adapt their firing frequency and favors the transition into a complete depolarization block with moderate currents. This also implies that besides serving as pacemakers, $Ca_v1.3$ LTCCs do also set the value of maximal current injection that the cell can handle.

SK dependent Na_V channel recovery is strongly attenuated in $Ca_v1.3^{-/-}$ MCCs

Na_V channels contribute specifically to the spike upstroke of the APs elicited in MCCs (Mahapatra et al., 2011). Na_V channel availability is reflected in the AP peak height, the V_{thresh} value and the velocity of the upstroke phase (dV/dt_{max}). We have previously shown that SK channels enhance the availability of Na_V channels at rest. Since $Ca_v1.3^{-/-}$ MCCs are less able to trigger SK currents, we reasoned that this should have severe consequences on Na_V channel recovery between induced APs. A possible gradual accumulation of Na_V channel inactivation might also partly explain the earlier switch into depolarization block of $Ca_v1.3^{-/-}$ MCCs. We thus compared AP waveforms triggered by 15 pA from V_h= -70 mV of WT (black), $Ca_v1.3^{-/-}$ (blue) and WT MCCs with apamin (red) (Fig. 6A). Data were derived from the AP waveforms shown in Fig. 4,5 and phase plane plots were obtained to measure the evolution of V_{thresh} and dV/dt_{max} (see above).

For WT MCCs we found a gradual reduction of both the AP peak amplitude and dV/dt_{max} while progressing from the first to the last spike of the AP-train. This effect on both parameters, however, could be considered moderate as compared to what observed for $Ca_v1.3^{-/-}$ and apamin-treated WT MCCs. The steady-state value of the AP peak in control conditions for WT MCCs (n= 23) was 6.6- and 2.5-fold bigger as compared to $Cav1.3^{-/-}$ (p< 0.001; n= 19; Fig. 6B left) and apamin-treated WT MCCs (p< 0.001; n= 18; Fig. 6B right), respectively. When applied to $Cav1.3^{-/-}$ MCCs, apamin had no significant effect on steady-state AP peaks as compared to control (5.6 ± 2.6 mV; n= 18 vs 2.7 ± 2.4 mV; n= 19) (data not shown). No significant differences were found between groups concerning AP peak amplitude at onset.

Data on dV/dt_{max} were in line with those for the peak amplitude (Fig. 6C). Cav1.3 deletion and SK block lead to 3.2 and 1.9-fold lower dV/dt_{max} steady-state values as compared to WT MCCs (Fig. 6C). Again steady-state dV/dt_{max} for $Cav1.3^{-/-}$ MCCs under control conditions (6.3 ± 1.3 V/s; n= 19) were found comparable to those under perfusion with apamin (6.6 ± 1.3 V/s; n= 18) (data not shown).

Finally, we compared V_{thresh} of the first and last AP of the train for WT (n= 23) and $Ca_v1.3^{-/-}$ MCCs (n= 19) in control and after SK block by apamin (Fig. 6D). V_{thresh} was obtained as described in Fig. 2. In WT and $Ca_v1.3^{-}$

$^{/-}$ MCCs, V_{thresh} shifted to more depolarized values during the last AP as compared to the first (from -29.1 to -28.5 mV for WT MCCs and from -27.7 to -24.8 mV for $Ca_V1.3^{-/-}$ MCCs) (Fig. 6D). Depolarization of V_{thresh} was significant ($p< 0.05$) only for the $Ca_V1.3^{-/-}$ MCCs. Apamin increased significantly V_{thresh} of the last AP of WT (-25.4 ± 0.7 mV; $p< 0.05$) but not of $Ca_V1.3^{-/-}$ MCCs (-25.5 ± 0.9 mV). All together these findings suggest that the availability of SK channels minimizes the reduction of the AP peak, the dV/dt_{max} and V_{thresh} observed in $Ca_V1.3^{-/-}$ MCCs. A reduced activation of SK channels in $Ca_V1.3^{-/-}$ MCCs is clearly reflected in the decreased ability to recover a sufficient amount of Na_V channels that are required to maintain persistent AP firings during sustained depolarization.

SK channels build up a subthreshold K^+ current which sets the duration of the interspike interval

Given the key role of SK in controlling SFA we next measured the time course of SK currents during evoked APs. SK currents underlying a train of APs, were measured in voltage-clamp using an AP-train command recorded from the same cell in current-clamp mode (Fig. 7A). Trains of APs were recorded during a 15 pA current injection of 700 ms, starting from a V_h of -70 to -80 mV. As for the slow tail current measurements (Fig. 1B-E), all current traces were obtained in the presence of 300 nM TTX and 1µM paxilline as control (black) and in the presence of apamin (red) to block the presumptive SK current (Fig. 7B). SK currents (blue traces) were obtained by subtracting control traces (black) from the apamin-resistant current (red trace in Fig. 7B). Strikingly, there was a robust SK current flowing during the three ISIs that progressively increased during the train (Fig. 7C).

Considering the SK current amplitude we found that maximal values were obtained during the spike upstroke and the repolarization phases at V_m between -20 and -10 mV (left and center insets in panel C). Interestingly, we observed also a dip in SK current at the AP peak that was associated with a decrease of SK conductance. This is evident when comparing the mean SK current at the last AP peak (22.7 pA at 22 mV; n= 13) with that during the 3rd ISI (18.7 pA at -38 mV; n= 18). With a K^+ reversal potential of -77 mV (Fig 1B) this corresponds to a conductance of 0.48 nS at the ISI and 0.22 nS at the peak. The almost 2-fold decrease of SK conductance at the AP peak is likely due to the SK channel's inwardly rectifying properties (Soh and Park, 2001; Li and Aldrich, 2011) and not to a sudden drop of cytosolic Ca^{2+} during the narrow AP peak (~0.5 ms). Cytosolic Ca^{2+} decays slowly, as reflected by the slow tail current kinetics (Park et al., 1996). In addition, SK channel deactivation occurs within 15-60 ms when Ca^{2+} is instantly removed (Hirschberg et al., 1998; Berkefeld et al., 2010; Adelman et al., 2012). SK channel closing is thus also too slow to sense any drop of

Ca^{2+} during an AP peak lasting <1 ms. The phenomenon of inward rectification was not further considered in this work.

Given the short duration of the spikes as compared to the ISIs we calculated the integral under the curve obtained after subtraction of the apamin trace from control (as shown in panel C) in order to obtain the net K^+ charge carried by open SK channels. The SK charge was then normalized to the cell capacitance (pC/pF). We observed SK charge densities that increased progressively during the AP train and were larger during the ISI (black bars, Fig. 7C right panel) with respect to the preceding spikes (dashed bars; $p< 0.05$). At ISI 3 the SK charge density was 4-fold larger than at spike 3 ($p< 0.001$; n= 13; Fig. 7C). It is thus evident that most of the SK current flows during the interspike potentials and only a very small fraction during the spike itself.

SK currents flowing during the interspike intervals are mainly $Ca_v1.3$-driven

Given that SK currents are sub-threshold currents that mainly sustain the ISIs and that SK-dependent SFA is strongly attenuated in the absence of $Ca_v1.3$, we next tested whether $Ca_v1.3$ was the main responsible VGCC for the ISI specific SK current. We have previously shown that the ISI is dominated by a prominent subthreshold $Ca_v1.3$ current, critical for MCC auto-rhythmicity (Marcantoni et al., 2010). Given that both $Ca_v1.3$ and SK currents show remarkable overlapping activation patterns during the ISI, a close relationship between both types of currents might exist. To test this, AP-clamp experiments were performed to study the Ca^{2+}-dependence of the apamin sensitive outward currents passing during the ISIs. As described before, APs were triggered by 700 ms pulses of 15 pA from V_h = -70 mV (Fig. 8 A,B). This lead to 3.5 ± 0.3 spikes in WT (n= 7) and 5.3 ± 0.3 spikes in $Ca_v1.3^{-/-}$ MCCs (n= 8). The resulting train of APs was subsequently used as voltage-clamp command to trigger the Ca^{2+}-driven apamin-sensitive outward currents that are mainly evident during the ISIs (black traces in Fig. 8A,B). LTCCs were blocked by 3 µM nifedipine (red traces, nife) while non-LTCCs (N, P/Q, R) were blocked by a mixture of 2 µM ω-agatoxin IVA, 3.2 µM ω-conotoxin GVIA and 400 nM SNX-482 (blue traces, tox) (Fig. 8B). In order to avoid contamination by BK or Na^+-activated K^+ currents, all traces were recorded in the presence of 300 nM TTX and 1 µM paxilline. Block of outward currents by apamin (green traces) was taken as evidence that the currents were SK channel operated.

Representative traces of the response of a WT MCC to L- and non-L-type blockers are given in Fig. 8B. The non-L-type blockers have nearly no effect on SK currents (blue trace) while nifedipine (red trace) fully blocks the outward current. Notice that the nifedipine trace closely overlaps with the apamin-resistant current (green trace) (Fig. 8B,D). This indicates that SK current build-up is strongly dependent on L-type currents. SK

charge densities with nifedipine (0.1 ± 0.03 pC/pF; n= 7) or apamin (0.1 ± 0.05 pC/pF; n= 7) in the bath (calculated by integrating the outward current in the interval from the AHP of the penultimate AP up to the V_{thresh} of the last AP) were significantly different from those calculated for control (0.42 ± 0.06 pC/pF; p< 0.001; n= 7) and toxin-resistant currents (0.37 ± 0.03 pC/pF; p< 0.001; n= 7), but not significantly different from each other (Fig. 8D). Most striking are the recordings from $Ca_v1.3^{-/-}$ MCCs, in which SK currents are clearly strongly attenuated and increase more weakly during the AP-train as compared to WT MCCs (Fig. 8B,C). SK currents in $Ca_v1.3^{-/-}$ MCCs are also slower in building up as compared to WT MCCs. We found that the total SK charge density during the last ISI of $Ca_v1.3^{-/-}$ MCCs (0.15 ± 0.03 pC/pF; n= 8) was 2.8 fold smaller than that of WT MCCs (0.42 ± 0.06 pC/pF; p< 0.001; n= 7) (black bars in Fig. 8D). Note that in $Ca_v1.3^{-/-}$ MCCs, the tiny SK outward currents remain Ca_v1 channel dependent, indicating partial contribution by $Ca_v1.2$ (Fig. 8B,D).

The calcium currents flowing during the interspike intervals are mainly Ca_v1 dependent

Given the crucial role of $Ca_v1.3$ LTCCs to allow SK currents to build up with time, we next tested for the contribution of L- and non-LTCCs to the total amount of Ca^{2+} that enters the cell during a train of APs (Fig. 8C). Solutions used contained 135 mM of TEA and 300 nM of TTX in the bath and 130 mM of Cs^+ in the pipette (see Materials and Methods). This implicates that no physiological APs could be evoked and urged us to use representative spike trains of WT and $Ca_v1.3^{-/-}$ MCCs for these experiments. The aforementioned Ca^{2+} channel blockers were tested on the total Ca^{2+} currents, final recordings were performed in the presence of 50 µM Cd^{2+} (grey traces) to uncover the remaining leakage current (Fig. 8C).

The most striking finding, evident from the representative Ca^{2+} current traces is the apparent lack of the slowly rising Ca^{2+} currents in the ISIs of the $Ca_v1.3^{-/-}$ MCCs as compared to WT MCCs (Fig. 8C). The area indicated was dissected into the spike and the ISI with its respective Ca^{2+} currents, illustrated in the insets. Considering the total Ca^{2+}-charge density that covers the last ISI and the last AP we found a significant 1.7-fold (p< 0.01) reduction for $Ca_v1.3^{-/-}$ MCCs (n= 8) as compared to WT's (n= 7) (Fig. 8E). Total Ca^{2+}-charge density was furthermore mainly LTCC-dependent for both WT and $Ca_v1.3^{-/-}$ MCCs, as indicated by the strong significant block by nifedipine (80% and 62% for WT's and $Ca_v1.3^{-/-}$'s respectively; p< 0.01) and the rather mild effect of the toxin mixture (Fig. 8E). The Ca^{2+}-charge density measured during the spike was strikingly similar between WT (n= 7) and $Ca_v1.3^{-/-}$ MCCs (n= 8) but major differences were found for the Ca^{2+}-charge that sustains the ISI (Fig. 8F,G). The values of these latter were drastically decreased by nearly 5-fold: from -0.13 ± 0.3 pC/pF (n= 7) to -0.02 ± 0.07 pC/pF; p< 0.001, n= 7). This ISI specific Ca^{2+} current was furthermore

completely blocked by nifedipine (91% block) in WT MCCs (Fig. 8G).

In conclusion, we observed a reduced flux of Ca^{2+} during the ISI, but not during the spike itself, that could be responsible for the reduction of the total Ca^{2+}-charge density in $Ca_v1.3^{-/-}$ MCCs with respect to WT MCCs (Fig. 8E,F,G). LTCCs are prominent also during the AP waveform, which might explain the prevailing block of nifedipine on the SK currents during trains of APs, even for $Ca_v1.3^{-/-}$ MCCs (Fig. 8). $Ca_v1.3$ deficiency drastically reduces the size of the total Ca^{2+}-charge that leads to smaller SK currents in $Ca_v1.3^{-/-}$ MCCs. It is not surprising that more spikes were needed for $Ca_v1.3^{-/-}$ MCCs in order to trigger a significant apamin-sensitive outward current that induces SFA. This gives convincing support that the reduced degree of SFA in $Ca_v1.3^{-/-}$ MCCs, which derives from the reduced SK currents, is driven by $Ca_v1.3$.

SK channels are not co-localized to a specific Ca^{2+} channel type

Given the strong nifedipine dependence of the SK current during spikes we next tested whether SK channels were indeed closely coupled to Ca_v1 channels in MCCs. We did this by measuring the Ca^{2+}-dependence of SK currents during controlled Ca^{2+} current injections in voltage-clamp mode. Specifically, we compared the block of Ca^{2+} currents with the corresponding block of SK tail currents by applying either 3 µM nifedipine (red traces) or a mixture of 2 µM ω-agatoxin IVA, 3.2 µM ω-conotoxin GVIA and 400 nM of SNX-482 (blue traces) to block L- or non L-type currents as shown before (Fig. 9A,B). Whole-cell Ca^{2+} currents were evoked by a 250 ms step depolarization to 0 mV from V_h= -50 mV (Fig. 9A), with 2 mM Ca^{2+} and 135 mM TEA in the bath and 130 mM Cs^+ in the pipette. Nifedipine blocked 54% of the total Ca^{2+} current with the remaining 46% being effectively blocked by the toxin mixture ($p< 0.001$; Fig. 9A inset), while Cd^{2+} induced full block (Fig. 9A). Next we tested the block of the slow tail currents by the same VGCC blockers (Fig. 9B). Slow tails were evoked as described before (Fig. 1D) using a 250 ms Ca^{2+} loading step to 0 mV followed by a 3 s lasting return step to -95 mV, repeated every 20 s at V_h= -50 mV (Fig. 9B top). We found that nifedipine blocked 58% of the total SK current (n= 15) while the remaining current (42%) was fully blocked by the toxin mixture (Fig. 9B inset). Apamin (200 nM) blocked ~88% of the total current (green trace) leaving a 5-10% residual current (Fig. 9B). Nearly full block of the slow tail currents (93%) was obtained by 50 µM Cd^{2+} with a residual slow tail current ≤ 5% of the total (Fig. 9B). The reduction of the slow tail current by nifedipine, toxin mixture, Cd^{2+} and apamin were all statistically significant as compared to control ($p< 0.05$) (Fig. 9B). This strong correlation between Ca^{2+} and SK current block suggests unequivocally that there is no preferential coupling of SK channels to any specific VGCC type in MCCs. We also found that lack of $Ca_v1.3$ does not lead to a significant decrease in SK current density as compared to WT (6.7 ± 2 pA/pC; n = 18 vs. -8.9 ± 1.3; $p> 0.05$;

n= 30) (not shown), proving that deficiency of Cav1.3 does not affect SK channel density.

To better assay for the absence of SK channel coupling to a specific Ca^{2+} source, slow tails were measured after loading MCCs with saturating concentrations (20 µM) of slow (EGTA-AM) and fast Ca^{2+} chelators (BAPTA-AM). Upon saturation, we washed with Tyrode's standard solution (Fig. 10C). Traces shown in Fig. 9C represent slow tails in Tyrode's standard after equilibrium was achieved. As shown, BAPTA-AM nearly abolished the slow tail current (80% block; $p< 0.01$; n= 7) while EGTA-AM significantly accelerated the time course of the current decay (Fig. 9C). In the latter case, SK tail currents were fitted with a double exponential with fast and slow time constants (τ_{fast}, τ_{slow}). EGTA nearly halved τ_{slow} (from 2.1 ± 0.3 s to 0.9 ± 0.1 s; $p< 0.01$; n= 5) leaving almost unaltered τ_{fast} (0.2 ± 0.03 s vs. 0.18 ± 0.03 s; $p> 0.05$; Fig 9C inset). In two cells we also applied 1 µM BayK 8644 in addition to BAPTA-AM with no evident differences (not shown). Given the high affinity of SK for Ca^{2+} (K_D= 0.5 µM) and the Ca^{2+} profile expected for 5 mM intracellular BAPTA (1 µM Ca^{2+} at 20-40 nm from the Ca^{2+} source) and EGTA (1 µM Ca^{2+} at 70-100 nm) our findings suggest that SK channels do not form specific micro-nano domains with VGCC's but are located at a distance sufficiently far from VGCC to allow EGTA to affect their Ca^{2+}-dependent activation (see below).

Discussion

We provided evidence in favor of a tonic $Ca_v1.3$-driven SK conductance that slows down MCC's basal firing rate and leads to spike frequency adaptation upon sustained current injections. $Ca_v1.3$ deficiency induces a nearly two-fold reduction of the total Ca^{2+} charge entering the cell due to a marked depression of the pacemaker current. This functional and not physical coupling to SK channels accounts for the inability of $Ca_v1.3^{-/-}$ MCCs to adapt their firing frequency. The uncovered "$Ca_v1.3$-SK interaction" guarantees an effective recovery of Na_V channels, required to maintain stable AP firings upon stimulation. $Ca_v1.3$ thus acts as "drive" and "brake" on MCC's excitability that could be crucial when controlling sustained catecholamine release from the adrenal gland during stressful stimuli (Garcia et al., 2006). This $Ca_v1.3$-mediated mechanism could also be critical to regulate the slow firing of some central neurons in which Ca_v1 channels help setting the pacemaker current (see Vandael et al., 2010).

SK channel expression and their role in firing at rest and during sustained membrane depolarization

The presence of SK currents in BCCs and RCCs has been established before by biophysical means but their role on MCCs pacemaker modulation remained elusive (Marty and Neher, 1985; Neely and Lingle, 1992;

Park, 1994). All three KCNN α-subunits were found to be expressed in MCCs giving rise to a bi-sigmoidal dose-response curve of apamin on slow tail currents. Different SK channel isoforms are characterized by distinct apamin sensitivities with SK2 being most sensitive (IC_{50}= 60-70 pM), SK3 showing an intermediate sensitivity (IC_{50}= 0.63-6 nM) and rat/mouse SK1 being rather insensitive (Ishii et al., 1997; Grunnet et al., 2001; Benton et al., 2003; D'hoedt et al., 2004; Weatherall et al., 2011). Heterologous expression studies (Ishii et al., 1997) have shown that SK channels might be heteromeric in nature, giving rise to channels with intermediate apamin sensitivities. The incomplete block by apamin together with the complex dose-response curve suggests that SK channels in MCCs might be heteromeric in origin. This assumption, however, requires further studies and raises the obvious question of why MCCs need such diverse SK channels with identical Ca^{2+}-sensitivity.

A strong negative correlation was found to exist between basal firing frequency and the percentage of frequency increase induced by apamin, which is strong evidence that firing of resting MCCs is tightly controlled by tonically active SK channels. Similarly, neurons from the lateral dorsal striatum that exhibit large SK currents respond with lower firing frequencies to current injections and show more pronounced responses to apamin as compared to neurons with less SK currents from the nucleus accumbens shell (Hopf et al., 2010). High basal firing frequencies (mild apamin effects) were furthermore correlated with low coefficients of variation in MCCs, indicating more regularity of the firing frequency with less SK channels and more irregularity with higher densities of SK channels. This is in contrast with findings on some central neurons where robust SK currents increase the regularity and precision of firing (Wolfart et al., 2001; Hallworth et al., 2003; Atherton and Bevan, 2005; Deister et al., 2009). The increased precision of firing, as seen by others, is due to an enhanced Na_V channel availability induced by SK channels that is required for pacemaking these cells. MCCs are not dependent on Na_V channels for their pacemaking (Mahapatra et al., 2011) but on LTCCs with low degree of inactivation ($Ca_V1.3$). This might explain the discrepancies with the aforementioned neuronal models.

Upon sustained current injections, SK channels in various neurons lead to SFA (Madison and Nicoll, 1984; Benda and Herz, 2003; Chen and Toney, 2009; Peron and Gabbiani, 2009; Lin et al., 2010; Vandecasteele et al., 2011). This holds as well for MCCs where SK channels slow-down the steady-state firing frequency. SK currents were shown to build-up during the ISIs, as occurs during bursts of APs in Purkinje neurons (Swensen and Bean, 2003). The fact that SK currents were surprisingly low during the AP peak might be related to SK channel's inwardly rectifying properties (Soh and Park, 2001; Li and Aldrich, 2011). SK inward

rectification likely avoids that this "voltage-insensitive" current shortcuts the AP upstroke and interferes with spike generation. SK channels are thus mainly conducting sub-threshold currents that show striking overlapping patterns with $Ca_v1.3$-dependent pacemaker currents of MCCs. The gradual increase of SK conductance will lower the cell's input resistance and gradually decrease the gain during steady-state firing frequencies due to the interference with the $Ca_v1.3$ specific depolarization throughout the ISI (Fig. 8C).

SK current accumulation responsible for SFA is driven by $Ca_v1.3$ in MCCs

$Ca_v1.3$ are known to be pacemaker channels in MCCs and to be tightly coupled to BK channels (Marcantoni et al., 2010). Their loss typically results in membrane depolarizations that lead to abnormally high-firing frequencies in the population of cells (20%) that maintained their spontaneous firing pattern. Loss of BK channels, however, leads to slower firing patterns in MCCs, in agreement with data on Purkinje neurons (Sausbier et al., 2004; Vandael et al., 2010). Interestingly, BK block during sustained current injections caused significant increases in the duration of the first interspike interval and fastened the onset of SFA (Vandael & Carbone, unpublished data). It is thus unlikely that loss of coupling to BK channels alone could account for the observed elevated firing frequencies of $Ca_v1.3^{-/-}$ MCCs. Here, we have unambiguously shown that ISI specific SK current accumulation during a train of spikes is strongly attenuated in $Ca_v1.3^{-/-}$MCCs.

Although block of LTCCs by nifedipine resulted in the complete block of SK-driven outward currents during the ISI, we did not reveal any molecular coupling between both channels (LTCCs vs. SK). Our data indicate that physiological protocols using APs can lead to distinct outcomes as when square pulses are used as voltage commands. While non-LTCCs contribute to half of the total Ca^{2+} charge flowing in the cell during controlled voltage steps we found that they only contribute to 20% of the total Ca^{2+} charge during a train of APs. High Ca^{2+}-sensitivity and voltage-independency of SK channels probably circumvent the requirement of a nanodomain organization between SK channels and their Ca^{2+} source (Fakler and Adelman, 2008). In agreement with this, we found that BAPTA fully blocks the SK tail currents while EGTA accelerates their decay. Assuming space constants (λ) of 20-40 nm for BAPTA and 70-100 nm for EGTA (Prakriya and Lingle, 2000), we estimated that SK channels cannot be closer than 40 nm and not far than 200 nm from VGCCs.

$Ca_v1.3$-driven SK channels increase Na_V channel availability and delay the onset of depolarization block

$Ca_v1.3$ deficiency, just like SK block, leads to fast firing patterns characterized by a gradual decrease of peak amplitude, dV/dt_{max} and a notable increase of V_{thresh}. Na^+ currents in chromaffin cells are mainly conducted by $Na_v1.7$ channels, characterized by a relatively slow recovery from fast inactivation (Wada et al., 2008).

MCCs are furthermore characterized by broad spikes where Na^+ current inactivation is ought to be rather complete at the end of the AP (Carter and Bean, 2009; Gittis et al., 2010). This underlines the importance of prolonging the duration and increasing the depth of the ISI to guarantee optimal Na^+ channel recovery, required to sustain AP upstrokes and stable AP shapes in MCCs. A role of SK channels in the recovery of Na_V channels from inactivation has been observed as well for GABAergic SNr neurons and globus pallidus neurons (Atherton and Bevan, 2005; Deister et al., 2009). Lower Na_V channel availability due to reduced SFA associated with $Ca_V1.3$ loss, or apamin application, resulted in earlier transitions into a depolarization block. This could explain why $Ca_V1.3^{-/-}$ MCCs typically responded with a train of high-frequency spikes followed by sustained depolarizations after LTCCs ($Ca_V1.2$) were boosted with BayK 8644 (Marcantoni et al., 2010; Vandael et al., 2010). These results agree with recent observations on RCCs that respond with similar depolarization blocks upon increased current injections when SK channels were blocked and fast inactivating BK channels were absent (as is the case for $Ca_V1.3^{-/-}$ MCCs) (Sun et al., 2009).

Functional implication on adrenal catecholamine secretion and Ca^{2+}-dependent neuronal firing

Our data indicate that $Ca_V1.3$/SK interactions in MCCs are critical in coping with strong input stimuli as is likely to occur during intense splanchnic nerve discharges. SK channels act as a “brake” to prevent over-excitation that could be critical in cells that fire slowly (~1 Hz) and rely on “Ca^{2+}-dependent pacemakers” such as chromaffin cells, dopaminergic and histaminergic neurons (Chan et al., 2007; 2010). The phasic response to sustained depolarization described here has clear-cut implications on the overall organization of catecholamine release in the adrenal medulla. The first is that increasing the frequency of stimulation does not necessarily lead to a linear increase of catecholamine secretion. Indeed, the catecholamine release induced by trains of electrical stimulations (0.1 to 30 Hz), reaches peak values between 3 and 10 Hz and then declines in rat and cat chromaffin cells (Wakade, 1981; Alamo et al., 1991; Montiel et al., 1995). The second implication is that, similarly to certain neuronal assemblies (Ladenbauer et al., 2012), the phasic response related to adaptation currents (e.g. SK) described here may help firing synchronization in the adrenal medulla where chromaffin cells are electrically coupled (Colomer et al., 2012). Synchronization followed by adaptation to low firing frequencies in extended areas of the adrenal medulla may optimize the release of catecholamines during intense prolonged stressful stimulation, preventing excessive accumulation of undesired levels of circulating catecholamines.

References

Adelman JP, Maylie J, Sah P (2012) Small-conductance Ca^{2+}-activated K^+ channels: form and function. Annu Rev Physiol 74:245-269

Alamo L, Garcia AG, Borges R (1991) Electrically-evoked catecholamine release from cat adrenals. Role of cholinergic receptors. Biochem Pharmacol 42(5):973-978

Atherton JF, Bevan MD (2005) Ionic mechanisms underlying autonomous action potential generation in the somata and dendrites of GABAergic substantia nigra pars reticulata neurons in vitro. J Neurosci 25(36):8272-8281

Benda J, Herz AV (2003) A universal model for spike- frequency adaptation. Neural Comput 15(11): 2523-2564

Benton DC, Monaghan AS, Hosseini R, Bahia PK, Haylett DG, Moss GW (2003) Small conductance Ca^{2+}-activated K^+ channels formed by the expression of rat SK1 and SK2 genes in HEK 293 cells. J Physiol 553(1):13-9

Berkefeld H, Fakler B, Schulte U (2010) Ca^{2+}- Activated K^+ channels: from protein complexes to function. Physiol Rev 90:1437-1459

Carabelli V, Marcantoni A, Comunanza V, de Luca A, Diaz J, Borges R, Carbone E (2007) Chronic hypoxia up-regulates α1H T-type channels and low-threshold catecholamine secretion in rat chromaffin cells. J Physiol 584(1):149-165

Carter BC, Bean BP (2009) Sodium entry during action potentials of mammalian neurons: incomplete inactivation and reduced metabolic efficiency in fast- spiking neurons. Neuron 64(6):898-909

Chan CS, Guzman JN, Llijic E, Mercer JN, Rick C, Tkatch T, Meredith GE, Surmeier DJ (2007) 'Rejuvenation' protects neurons in mouse models of Parkinson's disease. Nature 447(7148):1081-1086

Chan CS, Gertler TS, Surmeier DJ (2010) A molecular basis for the increased vulnerability of substantia nigra dopamine neurons in aging and Parkinson's disease. Mov Disord 25(1):S63-S70

Chen QH, Toney GM (2009) Excitability of paraventricular nucleus neurones that project to the rostral ventrolateral medulla is regulated by small-conductance Ca^{2+}-activated K^+ channels. J Physiol 587(17): 4235-4247

Colbert CM, Magee JC, Hoffman DA, Johnston D (1997) Slow recovery from inactivation of Na^+ channels underlies the activity-dependent attenuation of dendritic action potentials in hippocampal CA1 pyramidal neurons. J Neurosci 17(17):6512-6521

Colomer C, Martin AO, Desarménien MG, Guérineau NC (2012) Gap junction-mediated intercellular communication in the adrenal medulla: An additional ingredient of stimulus-secretion coupling regulation. Biochim Biophys Acta 1818(8):1937-1951

Cueni L, Canepari M, Lujan R, Emmenegger Y, Watanabe M, Bond CT, Franken P, Adelman JP, Luthi A. (2008) T-type Ca^{2+} channels, SK2 channels and SERCAs gate sleep-related oscillations in thalamic dendrites. Nat Neurosci 11(6):683-692

Deister CA, Chan CS, Surmeier DJ, Wilson CJ (2009) Calcium-activated SK channels influence voltage-gated ion channels to determine the precision of firing in globus pallidus neurons. J Neurosci 29(26):8452-8461

D'Hoedt D, Hirzel K, Pedarzani P, Stocker M (2004) Domain analysis of the calcium-activated potassium channel SK1 from rat brain. Functional expression and toxin sensitivity. J Biol Chem 279(13):12088-12092

Engbers JD, Anderson D, Asmara H, Rehak R, Mehaffey WH, Hameed S, McKay BE, Kruskic M, Zamponi GW, Turner RW (2012) Intermediate conductance calcium-activated potassium channels modulate summation of parallel fiber input in cerebellar Purkinje cells. Proc Natl Acad Sci U.S.A 109(7):2601-2606

Engel J, Schultens HA, Schild D (1999) Small conductance potassium channels cause an activity-dependent spike frequency adaptation and make the transfer function of neurons logarithmic. Biophys J 76(3):1310-1319

Faber ES (2009) Functions and modulation of neuronal SK channels. Cell Biochem Biophys 55(3):127-139

Fakler B, Adelman JP (2008) Control of K(Ca) channels by calcium nano/microdomains. Neuron 59(6):873-881

Garcia AG, Garcia-De-Diego AM, Gandia L, Borges R, Garcia-Sancho J (2006) Calcium signaling and exocytosis in adrenal chromaffin cells. Physiol Rev 56(4):1093-1131

Gettes LS, Reuter H (1974) Slow recovery from inactivation of inward currents in mammalian myocardial fibres. J Physiol 240(3):703-724

Gittis AH, Moghadam SH, du Lac S (2010) Mechanisms of sustained high firing rates in two classes of vestibular nucleus neurons: differential contributions of resurgent Na, Kv3, and BK currents. J Neurophysiol 104(3): 1625-1634

Grunnet M, Jespersen T, Angelo K, Frøkjaer-Jensen C, Klaerke DA, Olesen SP, Jensen BS (2001)

Pharmacological modulation of SK3 channels. Neuropharmacology 40(7):879-887

Hallworth NE, Wilson CJ, Bevan MD (2003) Apamin-sensitive small conductance calcium-activated potassium channels, through their selective coupling to voltage-gated calcium channels, are critical determinants of the precision, pace, and pattern of action potential generation in rat subthalamic nucleus neurons in vitro. J Neurosci 23(20):7525-7542

Hirschberg B, Maylie J, Adelman JP, Marrion NV (1998) Gating of recombinant small-conductance Ca-activated channels by calcium. J Gen Physiol 111(4):565-581

Hopf FW, Seif T, Mohamedi ML, Chen BT, Bonci A (2010) The small-conductance calcium-activated potassium channel is a key modulator of firing and long-term depression in the dorsal striatum. Eur J Neurosci 31(11):1946-1959

Ishii TM, Maylie J, Adelman JP (1997) Determinants of apamin and d-tubocurarine block in SK potassium channels. J Biol Chem 272(37):23195-23200

Jenerick H (1963) Phase plane trajectories of the muscle spike potential. Biophys J 3:363-377

Khaliq ZM, Bean BP (2010) Pacemaking in dopaminergic ventral tegmental area neurons: depolarizing drive from background and voltage-dependent sodium conductances. J Neurosci 30(21): 7401-7413

Korn SJ, Weight FF (1987) Patch-clamp study of the calcium-dependent chloride current in AtT-20 pituitary cells. J Neurophysiol 58(6):1431-1451

Koschak A, Reimer D, Huber I, Grabner M, Glossmann H, Engel J, Striessnig J (2001) α1D (Cav1.3) subunits can form L-type Ca^{2+} channels activating at negative voltages. J Biol Chem 276(25):22100-22106

Ladenbauer J, Augustin M, Shiau L, Obermayer K (2012) Impact of adaptation currents on synchronization of coupled exponential integrate-and-Fire neurons. PLoS Comput Biol 8(4):e1002478

Li W, Aldrich RW (2011) Electrostatic influences of charged inner pore residues on the conductance and gating of small conductance Ca^{2+} activated K^+ channels. Proc Natl Acad Sci U S A 108(15):5946-5953

Lin M, Hatcher JT, Chen QH, Wurster RD, Cheng ZJ (2010) Small conductance Ca^{2+}-activated K^+ channels regulate firing properties and excitability in parasympathetic cardiac motorneurons in the nucleus ambiguus. Am J Physiol Cell Physiol 299(6):C1285-1298

Madison DV, Nicoll RA (1984) Control of the repetitive discharge of rat CA1 pyramidal neurones in vitro. J Physiol 354:319-331

Mahapatra S, Marcantoni A, Vandael DH, Striessnig J, Carbone E (2011) Are Ca(v) 1.3 pacemaker channels

in chromaffin cells? Possible bias from resting cell conditions and DHP blockers usage. Channels (Austin) 5(3):219-224

Mangoni ME, Couette B, Bourinet E, Platzer J, Reimer D, Striessnig J, Nargeot J (2003) Functional role of L-type Cav1.3 Ca^{2+} channels in cardiac pacemaker activity. Proc Natl Acad Sci U S A 100(9):5543-5548

Marcantoni A, Vandael DH, Mahapatra S, Carabelli V, Sinnegger-Brauns MJ, Striessnig J, Carbone E (2010) Loss of Cav1.3 channels reveals the critical role of L-type and BK channel coupling in pacemaking mouse adrenal chromaffin cells. J Neurosci 30(2):491-504

Marion NV, Tavalin SJ (1998) Selective activation of Ca^{2+}-activated K^+ channels by co-localized Ca^2+ channels in hippocampal neurons. Nature 395(6705):900-905

Marty A, Neher E (1985) Potassium channels in cultured bovine adrenal chromaffin cells. J Physiol 367:117-141

Mercer JN, Chan CS, Tkatch T, Held J, Surmeier DJ (2007) Nav1.6 sodium channels are critical to pacemaking and fast spiking in globus pallidus neurons. J Neurosci 27(49):13552-13566

Montiel C, Lopez M.G, Sanchez-Garcia P, Maroto R, Zapater P, Garcia A.G. (1995) Contribution of SK and BK channels in the control of catecholamine release by electrical stimulation of the cat adrenal gland. J Physiol 486(2):427-437

Neely A, Lingle CJ (1992) Two components of calcium-activated potassium current in rat adrenal chromaffin cells. J Physiol 453:97-131

Novara M, Baldelli P, Cavallari D, Carabelli V, Giancippoli A, Carbone E (2004) Exposure to cAMP and beta-adrenergic stimulation recruits Ca(V)3 T-type channels in rat chromaffin cells through Epac cAMP-receptor proteins. J Physiol 558(2):433-449

Oliver D, Klocker N, Schuck J, Baukrowitz T, Ruppersberg JP, Fakler B (2000) Gating of Ca^{2+}-activated K^+ channels controls fast inhibitory synaptic transmission at auditory outer hair cells. Neuron 26(3):595-601

Park YB (1994) Ion selectivity and gating of small conductance Ca^{2+}-activated K^+ channels in cultured rat adrenal chromaffin cells. J Physiol 481(3):555-570

Park YB, Herrington J, Babcock DF, Hille B (1996) Ca^{2+} clearance mechanisms in isolated rat adrenal chromaffin cells. J Physiol 492(2):329-346

Peron S, Gabbiani F (2009) Spike frequency adaptation mediates looming stimulus selectivity in a collision-detecting neuron. Nat Neurosci 12(3):318-326

Platzer J, Engel J, Schrott-Fischer A, Stephan K, Bova S, Chen H, Zheng H, Striessnig J (2000) Congenital

deafness and sinoatrial node dysfunction in mice lacking class D L-type Ca^{2+} channels. Cell 102(1):89-97

Prakriya M, Lingle CJ (2000) Activation of BK channels in rat chromaffin cells requires summation of Ca^{2+} influx from multiple Ca^{2+} channels. J Neurophysiol 84(3):1123-1135

Sausbier M, Hu H, Arntz C, Feil S, Kamm S, Adelsberger H, Sausbier U, Sailer CA, Feil R, Hofmann F, Korth M, Shipston MJ, Knaus HG, Wolfer DP, Pedroarena CM, Storm JF, Ruth P (2004) Cerebellar ataxia and Purkinje cell dysfunction caused by Ca^{2+}-activated K^+ channel deficiency. Proc Natl Acad Sci U S A 101(25):9474-9478

Shah MM, Haylett DG (2002) K^+ currents generated by NMDA receptor activation in rat hippocampal pyramidal neurons. J Neurophysiol 87(6):2983-2989

Soh H, Park CS (2001) Inwardly rectifying current-voltage relationship of small-conductance Ca^{2+}-activated K^+ channels rendered by intracellular divalent cation blockade. Biophys J 80(5):2207-2215

Solaro CR, Lingle CJ (1992) Trypsin-sensitive, rapid inactivation of a calcium-activated potassium channel. Science 257(5077):1694-1698

Stocker M (2004) Ca^{2+}-activated K^+ channels: molecular determinants and function of the SK family. Nat Rev Neurosci 5(10):758-770

Sun L, Xiong Y, Zeng X, Wu Y, Pan N, Lingle CJ, Qu A, Ding J (2009) Differential regulation of action potentials by inactivating and noninactivating BK channels in rat adrenal chromaffin cells. Biophys J 97:1832-1842

Swensen AM, Bean BP (2003) Ionic mechanisms of burst firing in dissociated Purkinje neurons. J Neurosci 23(29):9650-9663

Vandael DH, Marcantoni A, Mahapatra S, Caro A, Ruth P, Zuccotti A, Knipper M, Carbone E. (2010) Ca(v)1.3 and BK channels for timing and regulating cell firing. Mol Neurobiol. 42(3):185-198

Vandecasteele M, Deniau JM, Venance L (2011) Spike frequency adaptation is developmentally regulated in substantia nigra pars compacta dopaminergic neurons. Neuroscience 192:1-10

Wada A, Wanke E, Gullo F, Schiavon E (2008) Voltage-dependent Na(v)1.7 sodium channels: multiple roles in adrenal chromaffin cells and peripheral nervous system. Acta Physiol (Oxf) 192(2):221-231

Wakade AR (1981) Studies on secretion of catecholamines evoked by acetylcholine or transmural stimulation of the rat adrenal gland. J Physiol 313:463-480

Weatherall KL, Seutin V, Liégeois JF, Marrion NV (2011) Crucial role of a shared extracellular loop in apamin

sensitivity and maintenance of pore shape of small-conductance calcium-activated potassium (SK) channels. Proc Natl Acad Sci U S A 108(45):18494-18499

Wolfart J, Neuhoff H, Franz O, Roeper J. (2001) Differential expression of the small-conductance, calcium-activated potassium channel SK3 is critical for pacemaker control in dopaminergic midbrain neurons. J Neurosci 21(10): 3443-3456

Xu W, Lipscombe D (2001) Neuronal Ca(V)1.3α_1 L-type channels activate at relatively hyperpolarized membrane potentials and are incompletely inhibited by dihydropyridines. J Neurosci 21(16):5944-5951

Figure legends

Fig 1. *SK channel expression, SK measurements by means of slow tail currents and their sensitivity to apamin*. **A,** RT-PCR performed on cDNA, after retro transcription of mRNA isolated from 6 mouse adrenal medulla's (M) and 3 mouse brains (B) (used as positive controls). (-) represents negative control, no cDNA was added. Specific bands can be observed for SK1 (564 bps), SK2 (354 bps), SK3 (590 bps) and BK (381 bps). N = 3 mice, done in triplicate. **B** slow tail current amplitudes plotted against the voltages at which tails were evoked. Right side shows voltage-clamp protocol and representative traces of a WT MCC bathed in 4 mM K^+ containing Tyrode solution. Blue line and triangles are recordings in a Tyrode with 6 mM K^+ (n= 4), red line and dots are recordings with 4 mM K^+ (n= 7), black line and squares represent recordings with 2 mM K^+ (n= 6). Data shown are not corrected for junction potential. **C,** apamin dose-response curve on slow tail currents evoked by 250 ms Ca^+ loading, measured at -95 mV in the presence of 12 mM K^+ in the bath. Data are expressed as % block vs. [apamin]. The continuous curve is a best fit with a double sigmoid function with saturating values at 66% (IC_{50} 0.3 nM)) and 82.8% (IC_{50} 80 nM). **D,** representative traces of SK currents in control condition (black), during application of 200 nM apamin (red) and 1 µM 1-EBIO (grey). *Top panel*: pulse protocol used. *Bottom panel*: mean current density at control (n= 39), with apamin (n= 39; *** p< 0.001) and with 1-EBIO (n= 6; *** p< 0.001). Degree of significance was determined by one-way ANOVA followed by a Bonferroni post-hoc analysis.

Fig 2. *SK channels slow-down spontaneous MCCs firing and are crucial for Na^+ channel recovery.* **A,** representative trace of the effect of 200 nM apamin on a spontaneously firing MCC (left). Averaged APs of 14 cells indicated by the black (control) and red (apamin) grids are shown overlapped to the right. **B,** Apamin induced a 3.4-fold increase in the mean spontaneous firing frequency (*** p< 0.001, paired Student's t-test). Basal firing frequency was plotted against the percentage increase of the frequency induced by apamin (n= 12). Linear regression using a maximum likelihood estimate with a correlation coefficient of -0.85. **C,** histogram distribution of the ISI duration in control (black, dashed) and during SK block by apamin (red), obtained from n= 12 cells. The top inset shows an example of the irregular firing pattern in control and more regular firing during apamin exposure. The bottom inset shows the decrease of the coefficient of variation (CV) induced by apamin (*** p< 0.001, paired Student's t-test). **D,** phase plane plots (dV/dt vs. V) from APs measured in control (black) and during apamin application (red) respectively. V_{thresh} was defined as the point where dV/dt reaches 4% of its maximal value (indicated as dV/dt_{max}). **E,** evolution of dV/dt_{max} during an AP-train in control conditions (black) and during SK block by apamin (red). Degree of significance was determined by a one-way ANOVA followed by a Bonferroni post hoc analysis (** p< 0.01; *** p< 0.001).

Fig 3. *Fast firing patterns associated with SK block lead to a progressive decline of TTX-sensitive Na^+ currents.* **A,** AP firing in control conditions (left, black) and during 200 nM apamin application (right, red) were used as voltage-clamp commands. **B,** current traces recorded in a control Tyrode solution containing 104 mM NaCl, 30 mM TEACl and 50 µM Cd^{2+} (black) and during application of 300 nM TTX (grey). **C,** subtraction of the traces in B results in the TTX-sensitive Na^+ current (blue). Insets in B are time scale expansions of the Na^+ currents at the time indicated by the arrow (3^{rd} AP). Inset in C shows the evolution of the Na^+ current amplitude during the command AP train in control (solid line) and during SK block by apamin (dotted line) (n=

9). Degree of significance was determined by a one-way ANOVA followed by a Bonferroni post-hoc analysis (* $p< 0.05$).

Fig 4. *SK-dependent spike frequency adaptation is strongly attenuated in $Ca_v1.3^{-/-}$ MCCs.* **A**, representative current-clamp responses for WT (left) and $Ca_v1.3^{-/-}$ MCCs (right) after 5, 10 or 15 pA current injection from V_h= -70 mV (from top to bottom). Traces in red at the bottom illustrate the effect of SK block by 200 nM apamin for WT and $Ca_v1.3^{-/-}$ MCCs after 15 pA current injection. **B (left),** mean values of f_O (white bars) and f_{SS} (black bars) in WT and $Ca_v1.3^{-/-}$ MCCs during 5, 10 and 15 pA current injection, obtained from n= 44, 67 and 56 WT MCCs respectively and from n= 51 and 28 $Ca_v1.3^{-/-}$ MCCs for 10 and 15 pA, respectively. **B (right),** comparison of the effect of apamin on f_O (white bars) and f_{SS} (black bars) between WT (n= 23) and $Ca_v1.3^{-/-}$ MCCs (n= 19) during 15 pA current injection. f_O was defined by the first interspike interval duration and f_{SS} by the last interspike interval duration as indicated in panel A (top). **C,** instantaneous firing frequency calculated at each ISI during 5 (light grey triangle), 10 (dark grey dots) and 15 pA (black squares) current injections in WT (left) and $Ca_v1.3^{-/-}$ MCCs (right). WT and $Ca_v1.3^{-/-}$ data were fitted by an exponential decay function with τ_{SFA} = 1 ± 0.3, 0.7 ± 0.1 and 0.9 ± 0.1 for 5, 10 and 15 pA in WT MCCs and τ_{SFA}= 0.9 ± 0.4 and 1.7 ± 0.4 for 10 and 15 pA in $Ca_v1.3^{-/-}$ MCCs, respectively. **D,** effect of SK block on the evolution of the instantaneous firing frequency in WT (left) and $Ca_v1.3^{-/-}$ MCCs (right) at 15 pA. Black squares represent control, red squares indicate the presence of apamin. WT-apamin and $Cav1.3^{-/-}$-apamin data were fitted by exponential decay functions with τ_{SFA}= 2 ± 0.7 and 1.5 ± 0.4, respectively. Degree of significance was determined by a one-way ANOVA followed by a Bonferroni post hoc analysis (* $p< 0.05$, ** $p< 0.01$ and *** $p< 0.001$).

Fig 5. *Loss of $Ca_v1.3$ and blockade of SK lead to reduced adaptation ratios and earlier onset of depolarization block*. **A,** representative voltage responses to increasing current injections of WT MCCs in control conditions (black traces, left) and upon perfusion with 200 nM apamin (red, middle) compared with $Ca_v1.3^{-/-}$ MCCs (blue, right). **B,** to the left are shown the adaptation ratios (f_O/f_{SS}) for current injections between 1 and 20 pA, comparing WT in control (black; n= 67) with WT MCCs treated with apamin (red; n= 42). To the right, are shown the adaptation ratios of WT and $Ca_v1.3^{-/-}$ MCCs (n= 51) for current steps of increasing intensity. Adaptation ratios were fitted with the following function $Y_0 + A_1 e^{(-x/\tau)}$ with Y_0, A_1 and τ as variables. The values of the variables for WT, WT with apamin and $Ca_v1.3^{-/-}$ fits were: 8, -7.6 ± 0.2, 11.7 ± 0.7 pA (R^2 = 0.94); 3, -3.09 ± 0.38, 1.7 ± 0.5 pA (R^2= 0.9) and 3, -3.1± 0.09, 1.6 ± 0.1 pA (R^2= 0.9), respectively. **C,** minimal amount of current required to elicit a train of APs (rheobase) was normally distributed for WTs as well as $Ca_v1.3^{-/-}$ MCCs. WT (dashed bars, black line) and $Ca_v1.3^{-/-}$ (blue bars, blue line) data were fit by a Gaussian function (R^2 = 0.95 for WT and 0.97 for $Ca_v1.3^{-/-}$) around a mean of 4.0 ± 0.2 pA and 6.6 ± 0.4 pA respectively ($p< 0.001$). **D and E,** onset of depolarization block for control WT (dashed bars, black line), apamin-treated WT (red bars, red line) and $Ca_v1.3^{-/-}$ MCCs (blue bars, blue line) were normally distributed and fit by Gaussian functions defined by an R^2 value of 0.73, 0.87 and 0.9, respectively. WT data were distributed around a mean of 19.5 ± 0.7 pA and were found to be significantly ($p< 0.001$) different from those of $Ca_v1.3^{-/-}$ MCCs (13.6 ± 0.6 pA) and WT MCCs treated with apamin (14.6 ± 0.5). Degree of significance was determined by a one-way ANOVA followed by a Bonferroni post-hoc analysis.

Fig 6. *Reduced degree of SK-dependent SFA of $Ca_v1.3^{-/-}$ MCCs is reflected in an increased degree of Na^+ channel inactivation and progressive changes of the AP waveform.* **A,** overlap of APs, together with their respective phase plane plots (dV/dt vs. V) retrieved from a spike train triggered by 15 pA current injection for WT MCCs (black, top), $Ca_v1.3^{-/-}$ MCCs (blue, middle) and WT MCCs perfused with apamin (red, bottom). **B,** evolution of the peak amplitude with time for WT (black squares), $Ca_v1.3^{-/-}$ (blue dots) and WT MCCs perfused with apamin (red triangles) (*** p< 0.001). **C,** same as for B but taking into consideration dV/dt_{max} (** p< 0.01; *** p< 0.001). **D,** Comparison of V_{thresh} in control (black bars) and during apamin application (red) between the first- and the last AP of the spike train for WT MCCs (left) and $Ca_v1.3^{-/-}$ MCCs (right) (* p< 0.05). Degree of significance was determined by a one-way ANOVA followed by a Bonferroni post-hoc analysis.

Fig 7. *SK currents build-up during the interspike intervals at sub-threshold potentials.* **A,** train of APs from a representative WT MCC recorded after 15 pA current injection of 700 ms, starting from V_h= -70 mV. This trace was subsequently used as voltage-clamp command to reveal the SK currents on the same cell. **B,** all current traces were obtained in the presence of 300 nM TTX and 1 µM paxilline as control (black) and in the presence of 200 nM apamin (red) to block the presumptive SK current. **C,** SK currents (blue) obtained after subtraction of the apamin trace from the control trace of panel B. The two rectangles show time scale expansions of the blue trace from the second and third AP, as indicated. *Right inset*: SK charge density (pC/pF) obtained by integrating the area under the curve of the SK current as shown in panel C. Mean SK charge densities flowing during the spike (indicated by the grey area in the insets) are given as dashed bars, those flowing during the following ISI are shown as black bars. Significant differences were obtained by one-way ANOVA followed by a Bonferroni post-hoc analysis (* p< 0.05, ** p< 0.01 and *** p< 0.001).

Fig 8. *The absence of interspike specific Ca^{2+} currents leads to a strongly attenuated SK current built-up in $Ca_v1.3^{-/-}$ MCCs.* **A,** Representative train of APs from a WT (left) and $Ca_v1.3^{-/-}$ MCC (right) recorded after a 15 pA (700 ms) current step starting from V_h= -70 mV. The voltage traces were used as voltage-clamp command to reveal the interspike specific apamin-sensitive currents. **B,** representative Ca^{2+} and K^+ currents recorded in control condition (black trace) and in the presence of either 3 µM nifedipine (red), a toxin mixture (2 µM ω-Aga IVA, 3.2 µM ω-Ctx GVIA, 400 nM SNX-482) (blue) or 200 nM apamin (green). The control solution was a Tyrode standard (2 mM Ca^{2+}, 4 mM K^+) containing 300 nM TTX and 1 µM paxilline. **C,** representative Ca^{2+} currents covering the interspike interval of WT (left) and $Ca_v1.3^{-/-}$ MCCs (right). External solution contained 135 mM TEA, 300 nM TTX and 2 mM Ca^{2+}. Colored traces have the same meaning as in panel B. The grey traces were recorded in the presence of 50 µM Cd^{2+} and the cyan traces represent the time course of SK currents**. C,** left and right insets show on an expanded time scale the Ca^{2+} currents flowing during the spike and the ISI of WT and $Ca_v1.3^{-/-}$ MCCs, respectively. **D,** Comparison of the SK charge density covering the last ISI between WT and $Ca_v1.3^{-/-}$ MCCs. Blockers are represented by the same colors used in panel B. **E,** L- and non-LTCC dependency of the total Ca^{2+}-charge density (spike + ISI) of WT and $Ca_v1.3^{-/-}$ MCCs. **F-G,** same as for E but separating the Ca^{2+}-charge covering the spike and the ISI, respectively. Significant differences were obtained by one-way ANOVA followed by a Bonferroni post-hoc analysis (* p< 0.05, ** p< 0.01 and *** p< 0.001).

Fig 9: *SK channels are not coupled to any particular VGCC, but rather reside in nearby micro-domains*. **A,** to the left are shown representative Ca^{2+} currents evoked by the pulse protocol given on top. Control solution

contained 2 mM Ca^{2+}, 135 mM TEA and 300 nM TTX (black trace). Red, blue and grey traces were recorded in the presence of 3 µM nifedipine, a toxin mixture (2 µM ω-Aga IVA, 3.2 µM ω-Ctx GVIA, 400 nM SNX-482) and 50 µM Cd^{2+}, respectively. Colored bars to the right are mean peak current densities (pA/pF) derived from n= 13 cells. The inset represents the percentage contribution of L- (black) and non-LTCCs (white) to the total current. **B,** representative slow tail currents (left) evoked by the pulse protocol given on top. The control solution contained 2 mM Ca^{2+}, 12 mM K^{+}, 1 µM paxilline and 300 nM TTX (black trace). Colored bars to the right are mean current densities (pA/pF) derived from n= 15 cells. Ca^{2+} channel blockers were used as described for panel A. The green trace and bar were obtained with 200 nM apamin. Inset shows the percentage contribution of L- (black) and non-LTCCs (white) to the total slow tail current. **C,** the SK control current is represented by the black trace. Red and blue traces were recorded following cell loading with EGTA-AM (20 µM) and BAPTA-AM (20 µM), respectively. Bars to the right are the mean current densities of n=7 cells. Black and white continuous lines overlapping EGTA-AM and control traces represent double exponential fits of slow tails. Inset compares slow decay time constant at control (white) with EGTA-AM (black). **C inset**, significant differences were obtained by a paired student t-test with ** $p< 0.01$. **A-C**, Significant differences were obtained by a one-way ANOVA followed by a Bonferroni post hoc analysis (* $p< 0.05$, ** $p< 0.01$ and *** $p< 0.001$).

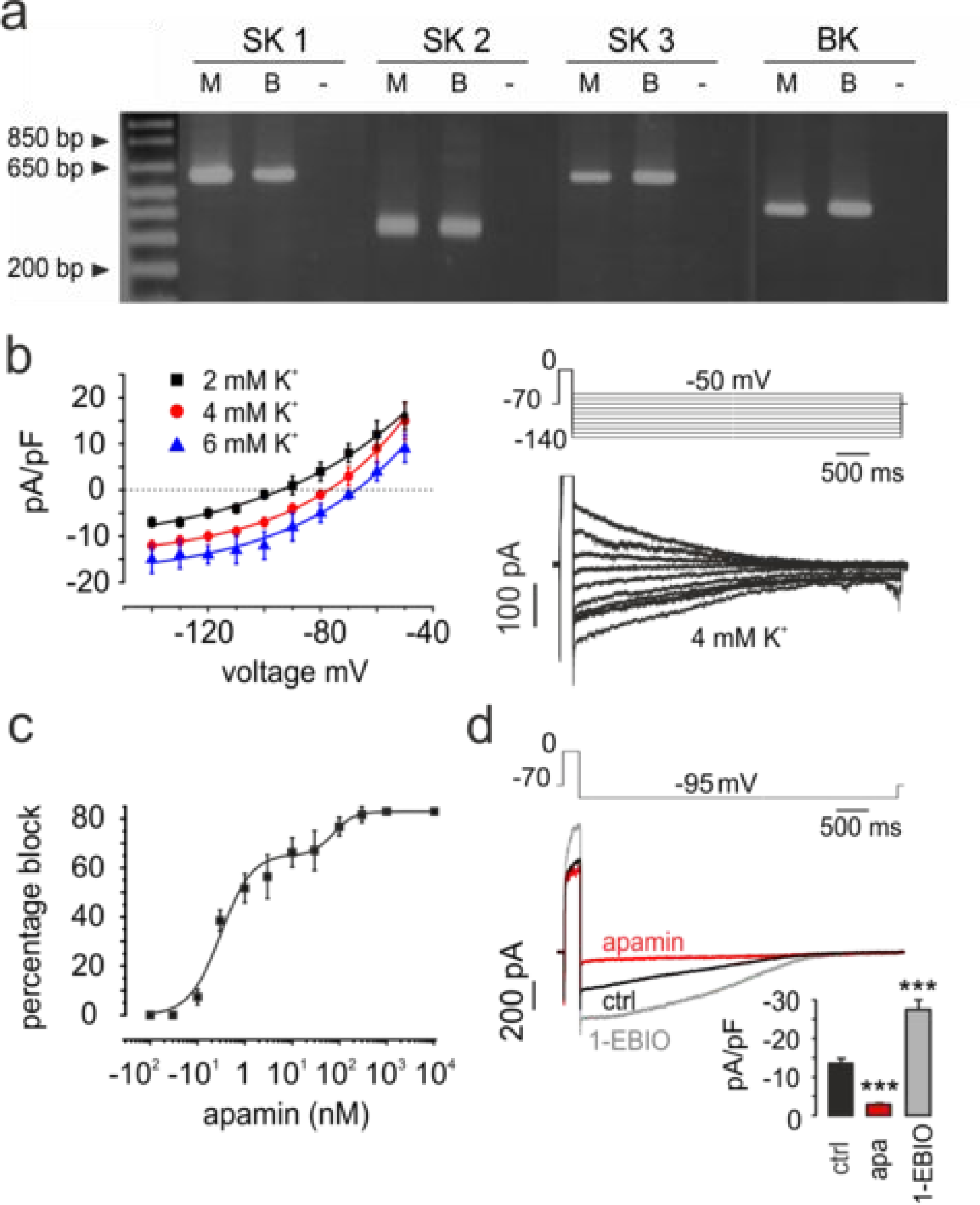
a
SK 1
SK 2
SK 3
BK
M
B
-
850 bp
650 bp
200 bp
b
2 mM K+
4 mM K+
6 mM K+
pA/pF
20
10
0
-10
-20
-120
-80
-40
voltage mV
0
-70
-140
-50 mV
500 ms
100 pA
4 mM K+
c
percentage block
80
60
40
20
0
-10² -10¹ 1 10¹ 10² 10³ 10⁴
apamin (nM)
d
0
-70
-95 mV
500 ms
200 pA
apamin
ctrl
1-EBIO
pA/pF
-30
-20
-10
0
***
***
ctrl
apa
1-EBIO

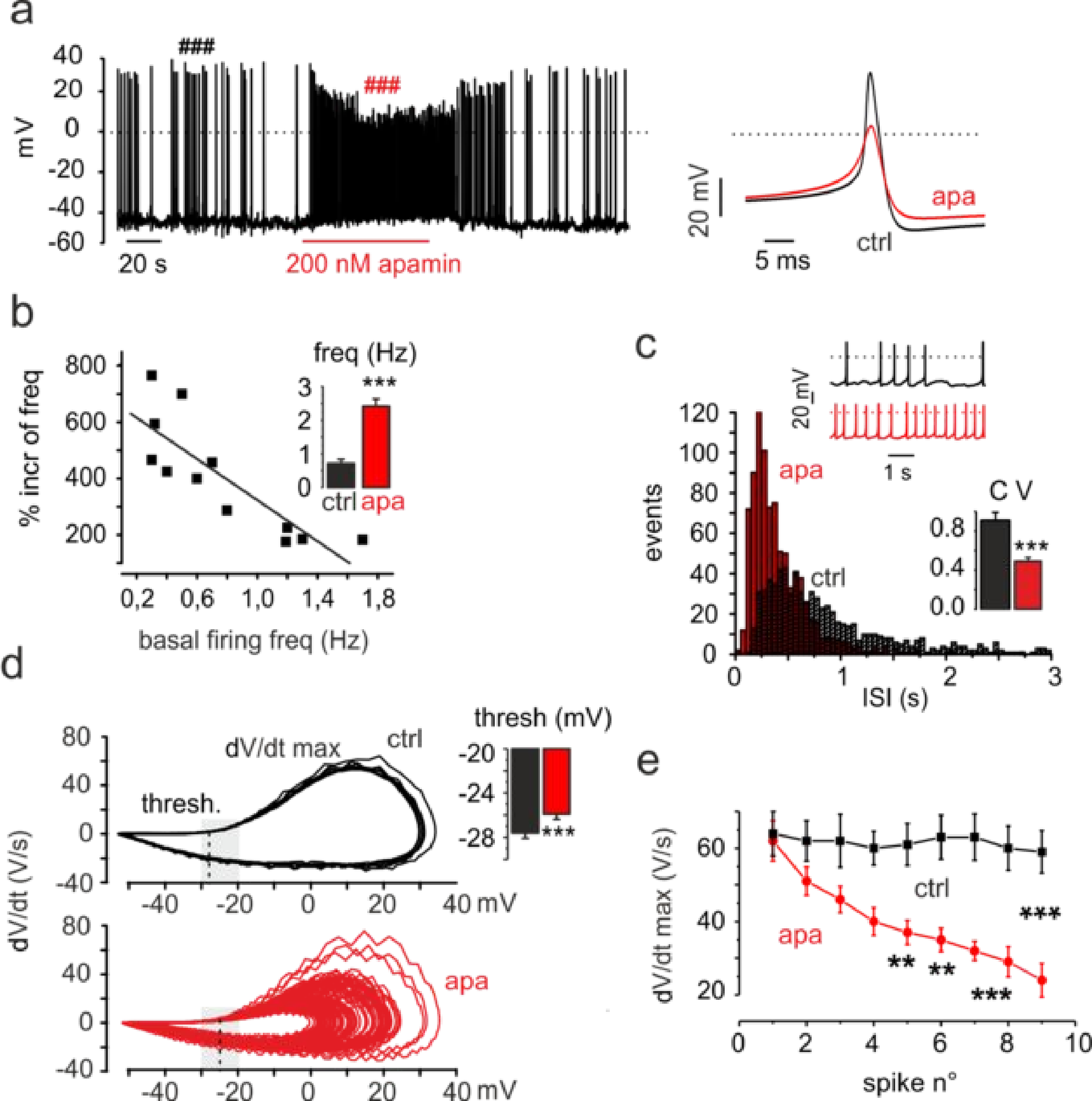
a
###
###
40
20
0
-20
-40
-60
mV
20 s
200 nM apamin
20 mV
5 ms
ctrl
apa
b
% incr of freq
800
600
400
200
0,2
0,6
1,0
1,4
1,8
basal firing freq (Hz)
freq (Hz)
3
2
1
0
***
ctrl
apa
c
20 mV
1 s
apa
ctrl
events
120
100
80
60
40
20
0
0
1
2
3
ISI (s)
C V
0.8
0.4
0.0
***
d
dV/dt (V/s)
80
40
0
-40
dV/dt max
ctrl
thresh.
-40
-20
0
20
40 mV
thresh (mV)
-20
-24
-28
***
apa
e
dV/dt max (V/s)
60
40
20
ctrl
apa
***
**
**
***
0
2
4
6
8
10
spike n°

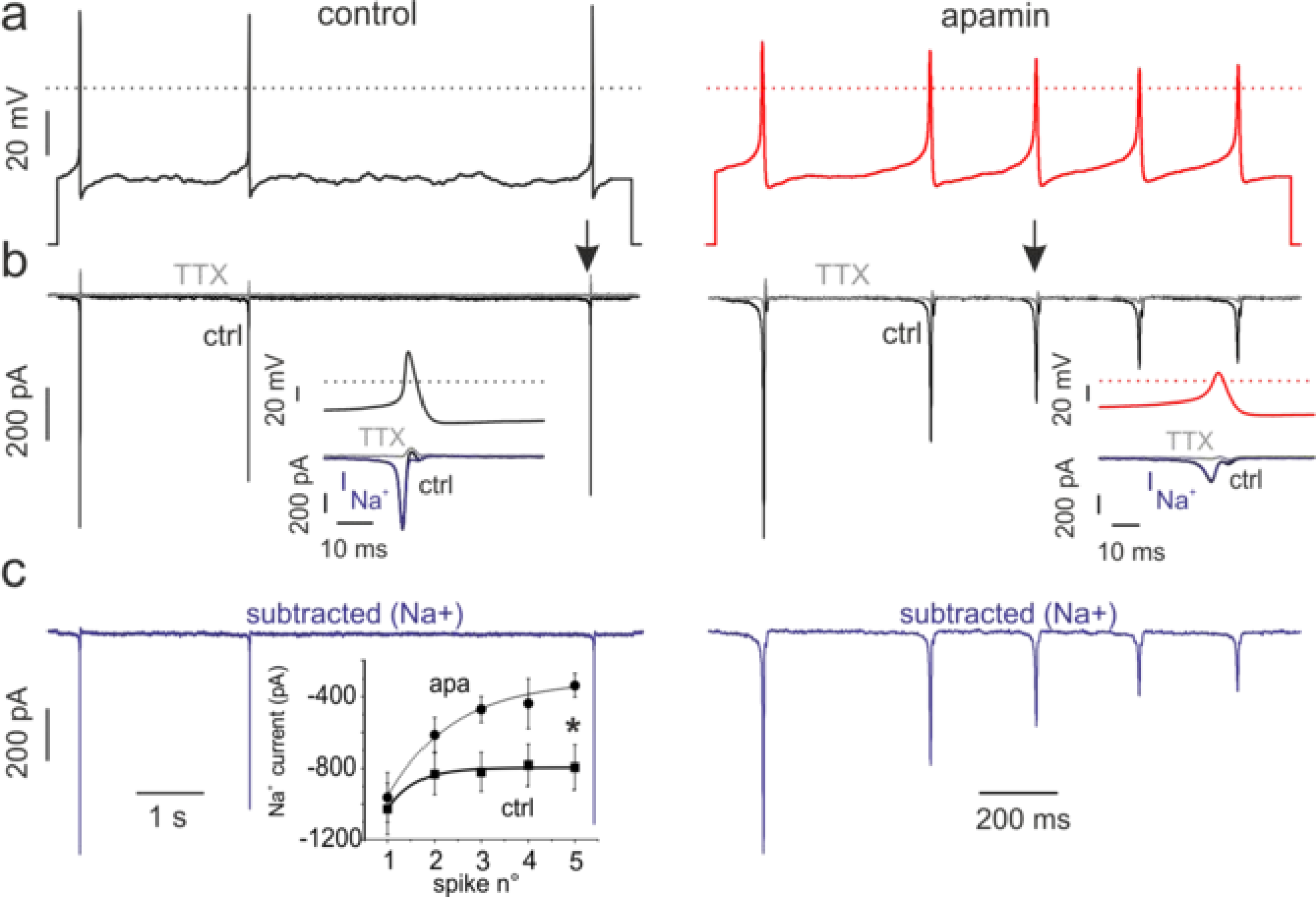
a
control
apamin
20 mV
b
TTX
ctrl
200 pA
20 mV
TTX
200 pA
I Na+
ctrl
10 ms
TTX
ctrl
20 mV
TTX
200 pA
I Na+
ctrl
10 ms
c
subtracted (Na+)
200 pA
1 s
Na+ current (pA)
-400
-800
-1200
apa
ctrl
*
1
2
3
4
5
spike n°
subtracted (Na+)
200 ms

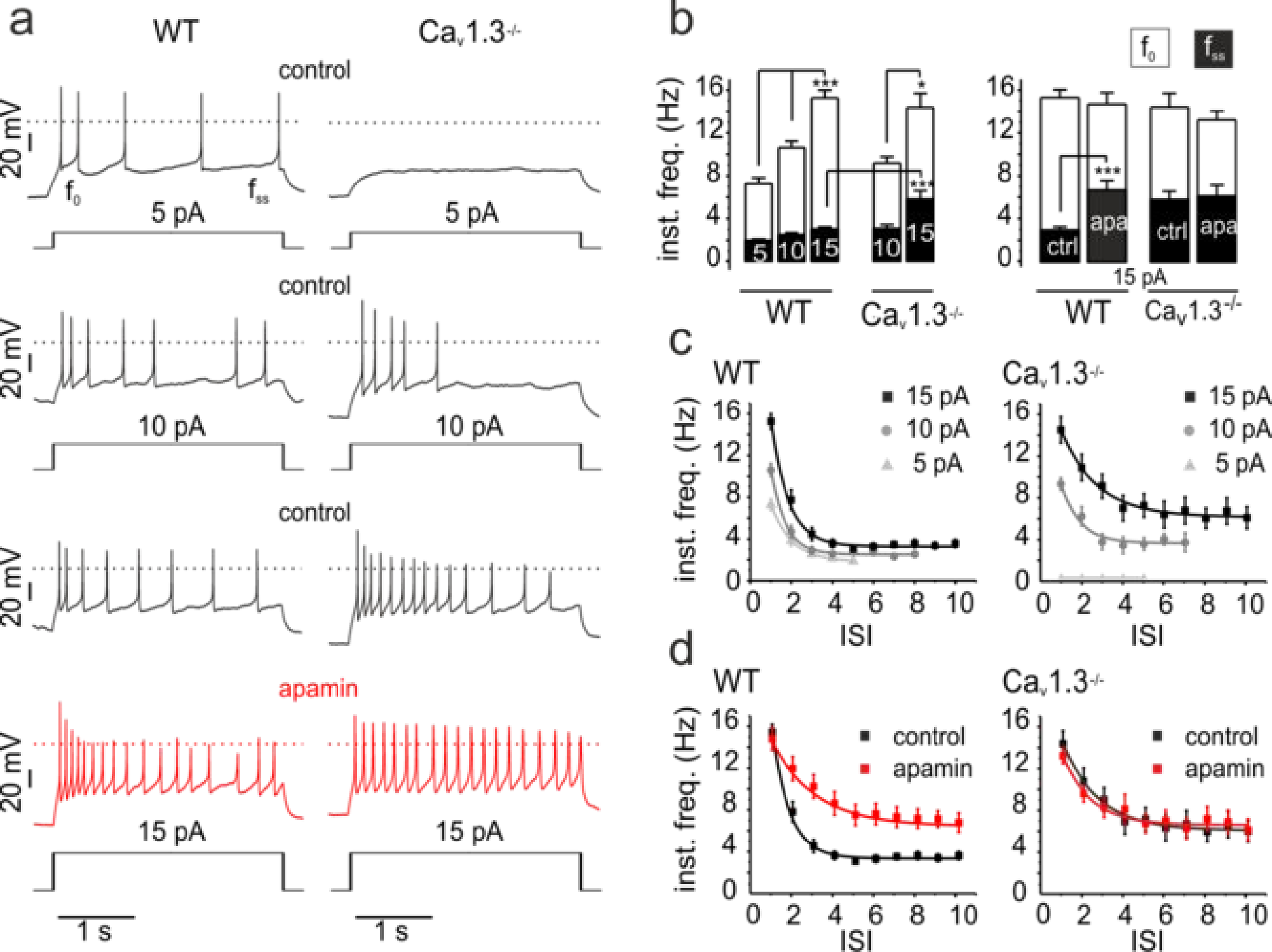
a
WT
Cav1.3-/-
control
20 mV
f0
fss
5 pA
control
10 pA
control
apamin
15 pA
1 s
b
f0
fss
inst. freq. (Hz)
***
*
5
10
15
ctrl
apa
WT
Cav1.3-/-
c
WT
Cav1.3-/-
15 pA
10 pA
5 pA
inst. freq. (Hz)
ISI
d
control
apamin

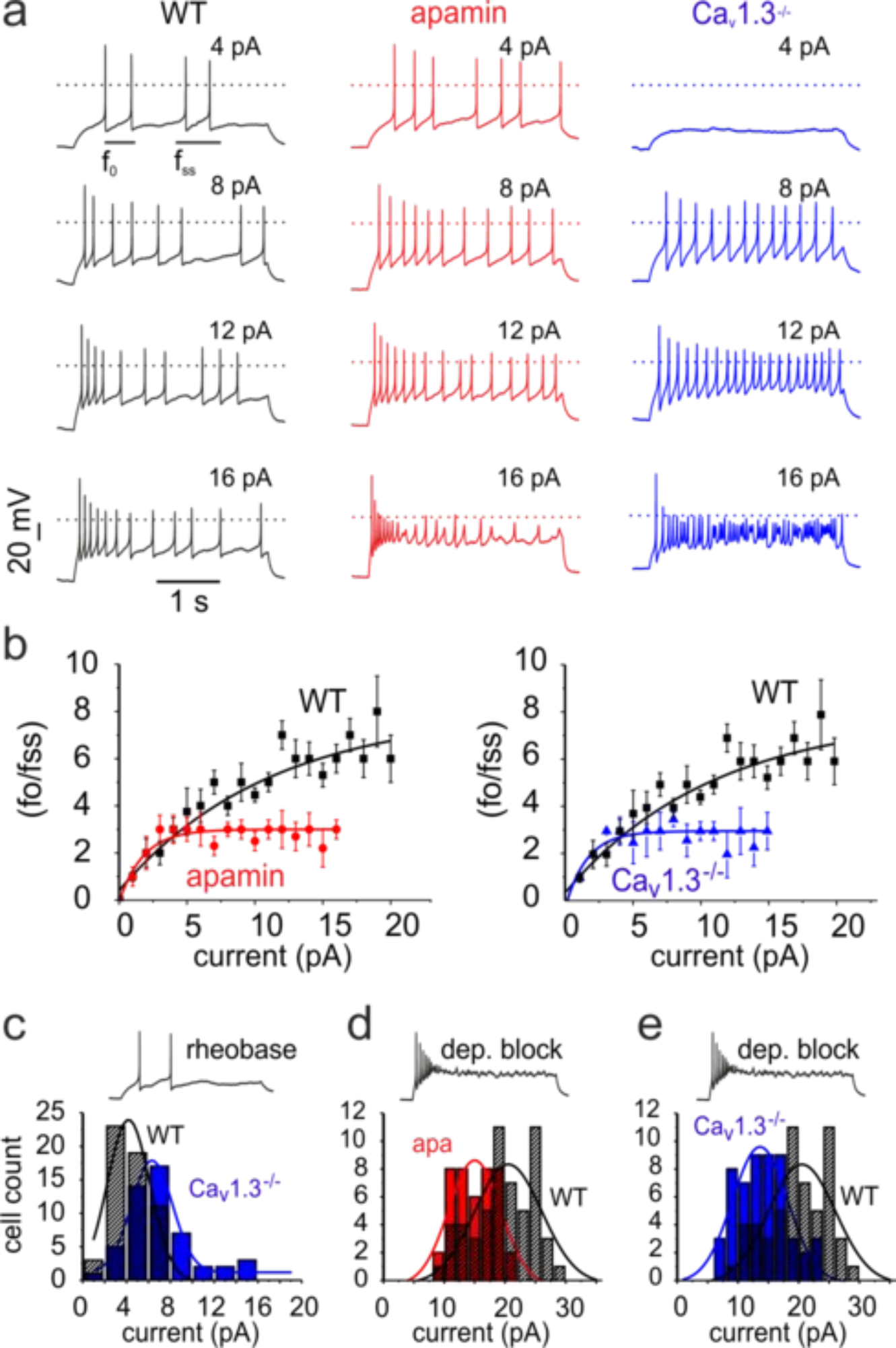
a
WT
apamin
Cav1.3-/-
4 pA
8 pA
12 pA
16 pA
f0
fss
20 mV
1 s
b
(fo/fss)
current (pA)
WT
apamin
Cav1.3-/-
c
rheobase
cell count
d
dep. block
apa
e
dep. block

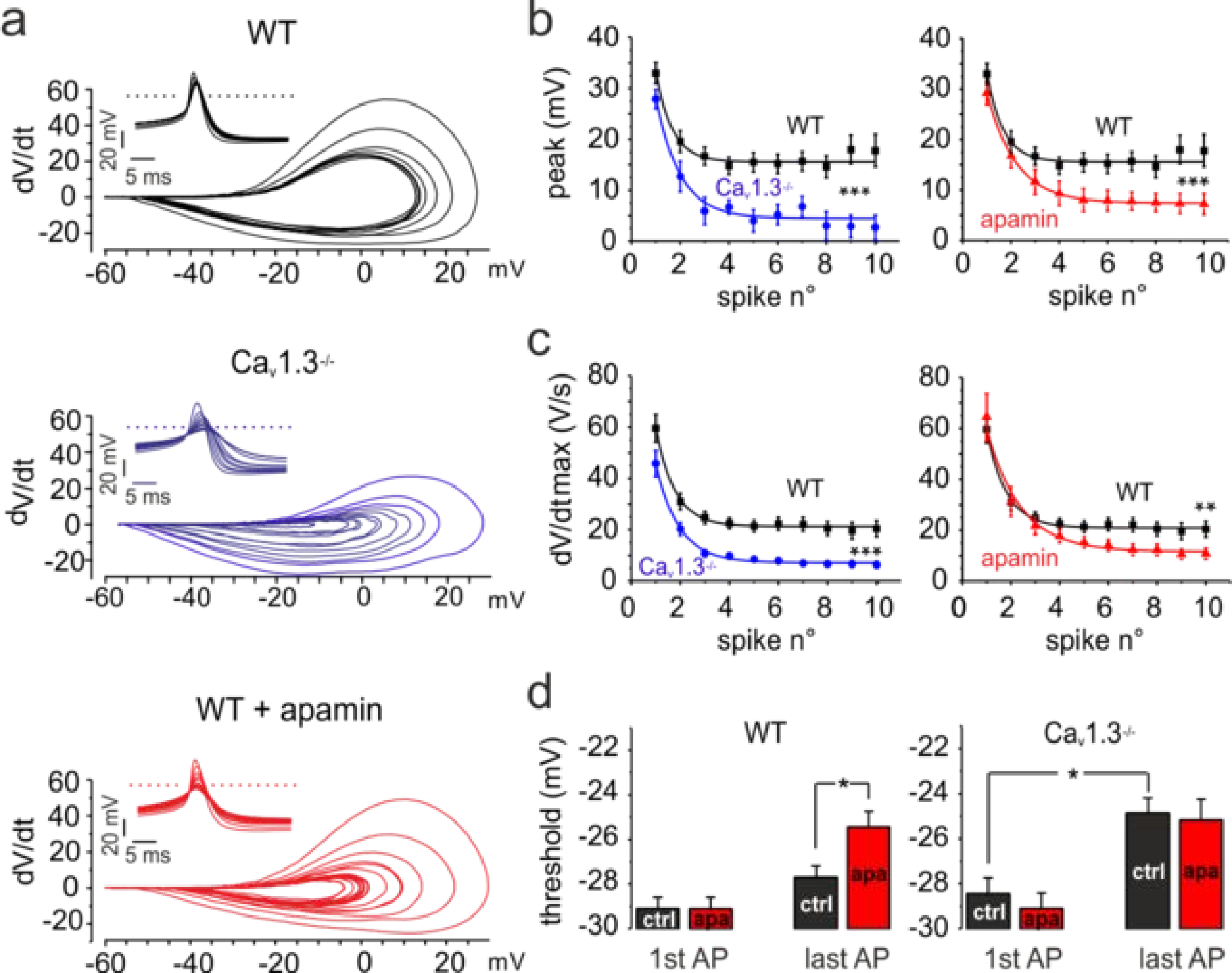
a
WT
dV/dt
20 mV
5 ms
mV
Ca$_v$1.3$^{-/-}$
WT + apamin
b
peak (mV)
spike n°
WT
Ca$_v$1.3$^{-/-}$
apamin
***
c
dV/dtmax (V/s)
**
d
threshold (mV)
ctrl
apa
1st AP
last AP
*

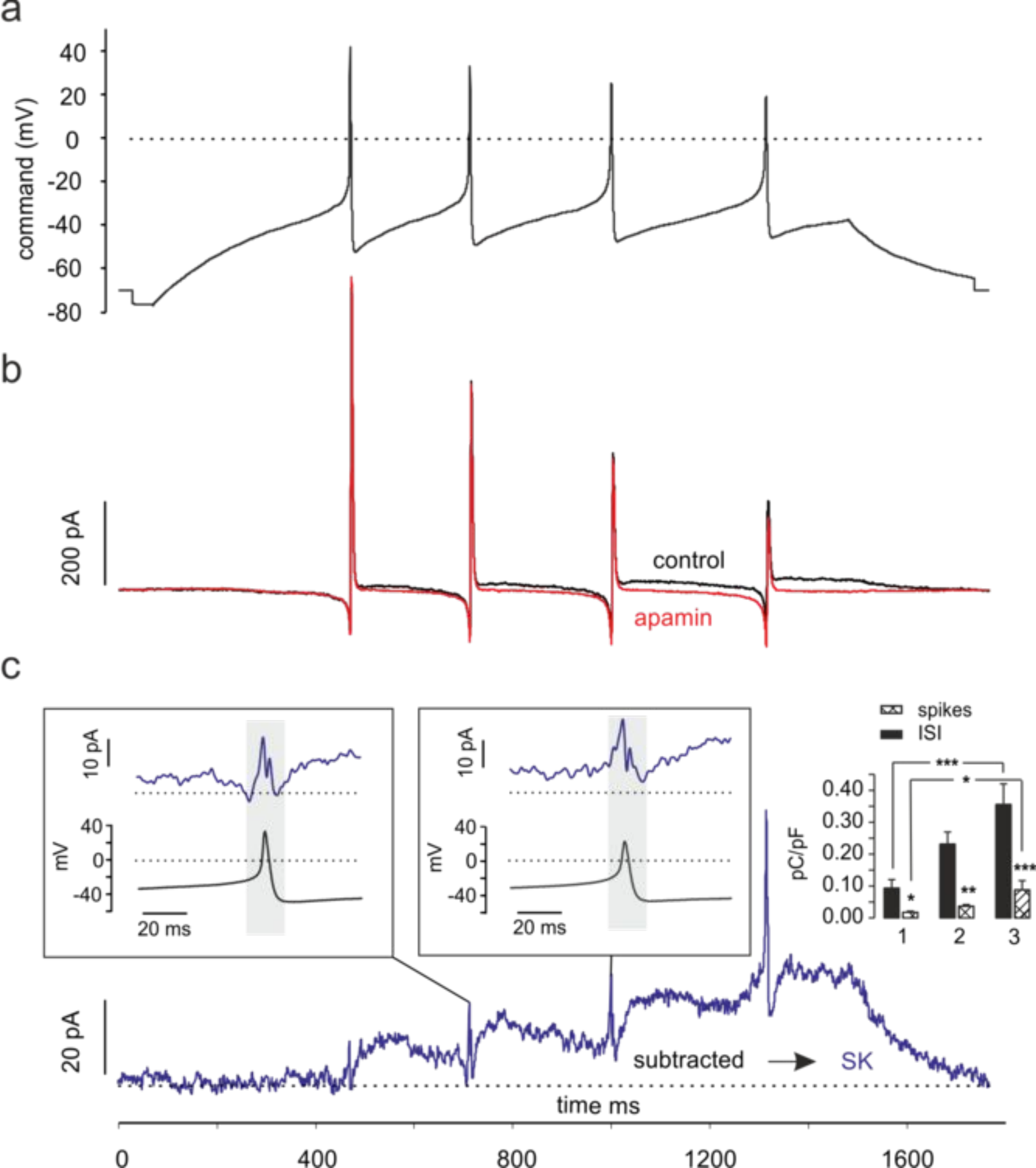
a
40
20
0
-20
-40
-60
-80
command (mV)
b
200 pA
control
apamin
c
10 pA
40
0
-40
mV
20 ms
10 pA
40
0
-40
mV
20 ms
spikes
ISI
***
*
0.40
0.30
0.20
0.10
0.00
pC/pF
*
**
***
1
2
3
20 pA
subtracted
SK
time ms
0
400
800
1200
1600

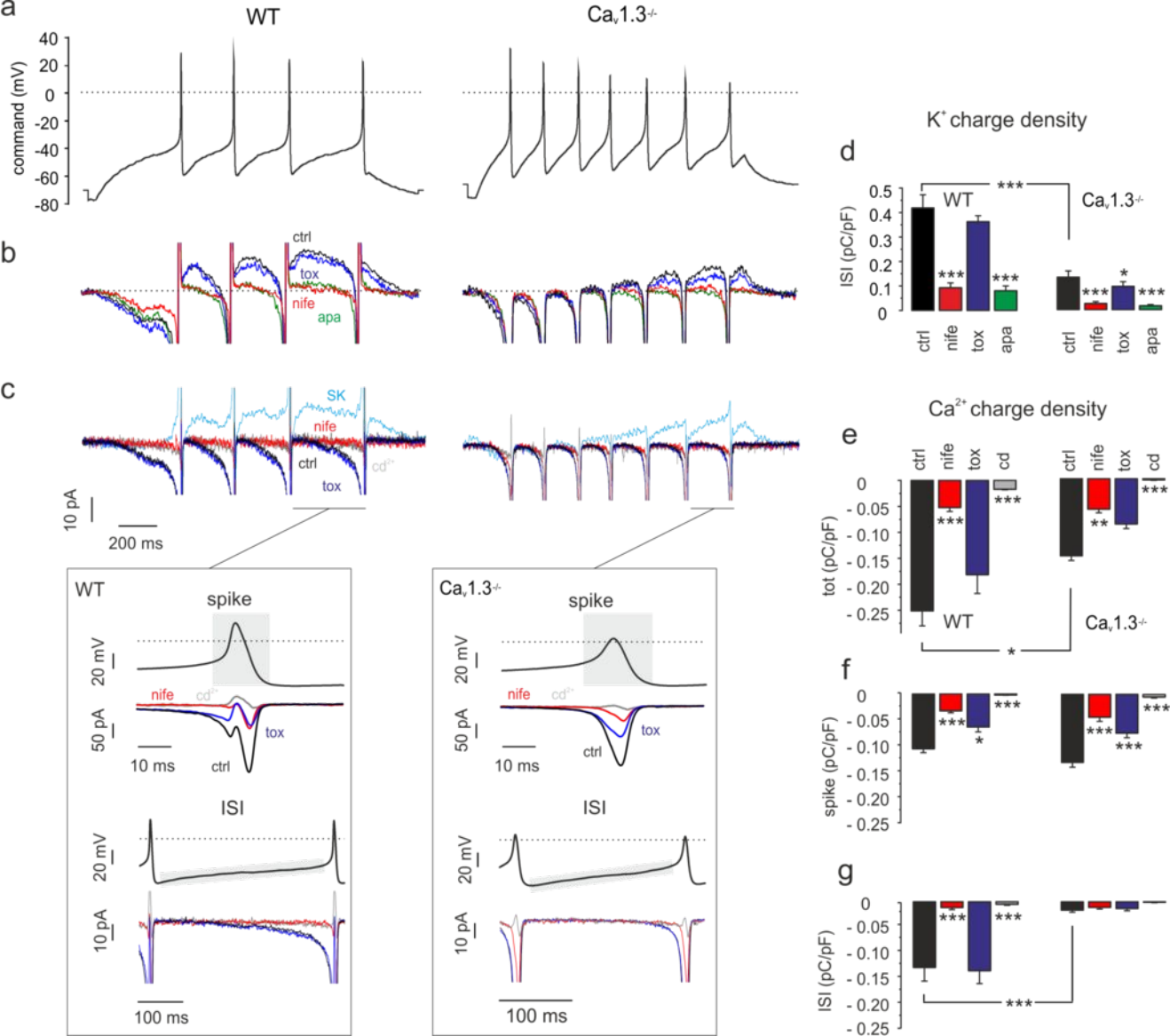
a
WT
Cav1.3-/-
command (mV)
40
20
0
-20
-40
-60
-80
b
ctrl
tox
nife
apa
c
SK
nife
ctrl
tox
cd2+
10 pA
200 ms
WT
spike
20 mV
50 pA
nife
cd2+
tox
10 ms
ctrl
ISI
20 mV
10 pA
100 ms
Cav1.3-/-
spike
20 mV
50 pA
nife
cd2+
tox
10 ms
ctrl
ISI
20 mV
10 pA
100 ms
d
K+ charge density
ISI (pC/pF)
0.5
0.4
0.3
0.2
0.1
0
WT
Cav1.3-/-
***
***
***
***
*
***
ctrl
nife
tox
apa
ctrl
nife
tox
apa
e
Ca2+ charge density
tot (pC/pF)
0
- 0.05
- 0.10
- 0.15
- 0.20
- 0.25
ctrl
nife
tox
cd
ctrl
nife
tox
cd
***
***
**
***
WT
Cav1.3-/-
*
f
spike (pC/pF)
0
- 0.05
- 0.10
- 0.15
- 0.20
- 0.25
***
*
***
***
***
g
ISI (pC/pF)
0
- 0.05
- 0.10
- 0.15
- 0.20
- 0.25
***
***
***

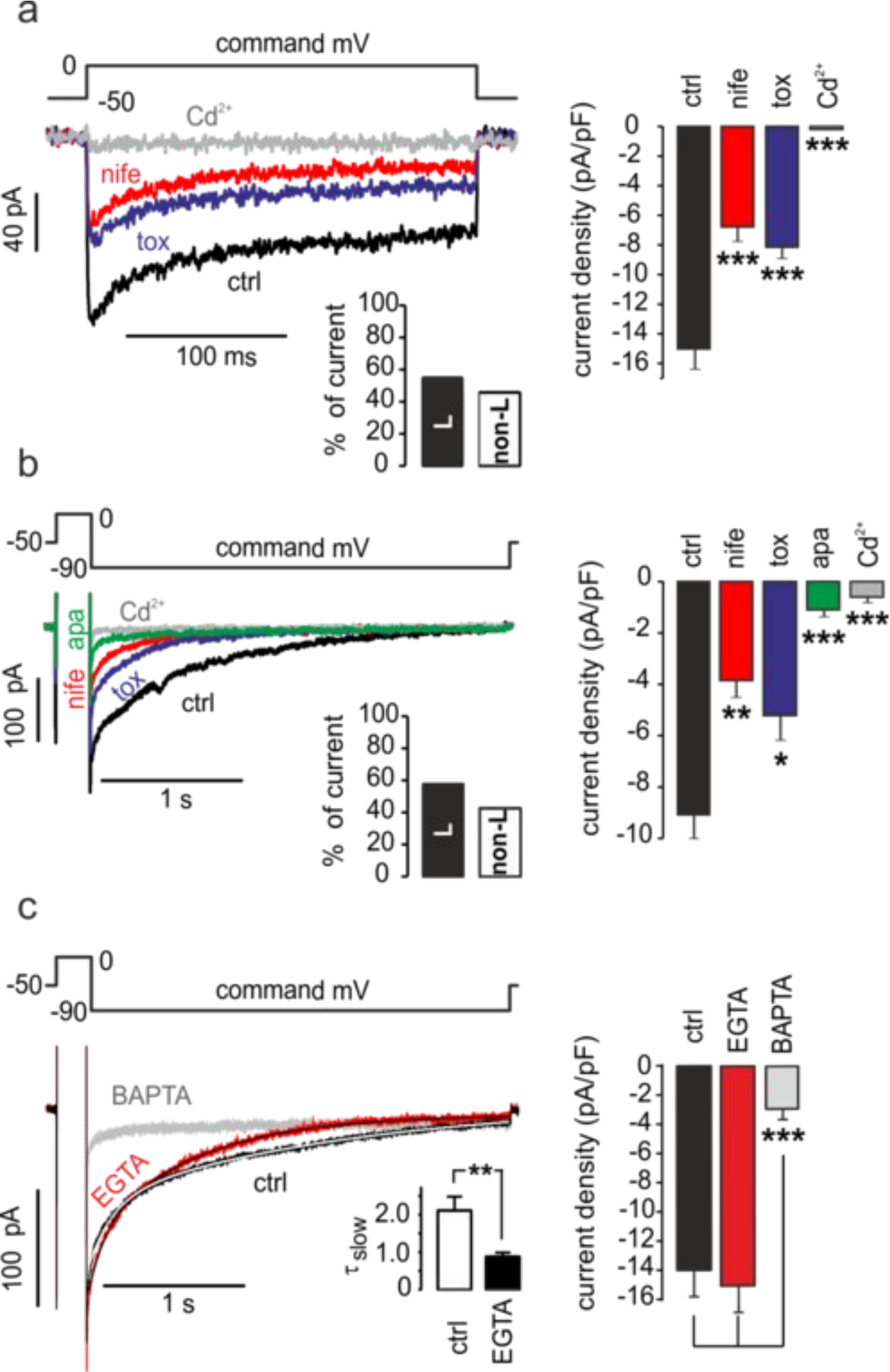
a
command mV
0
-50
Cd2+
nife
tox
ctrl
40 pA
100 ms
% of current
100
80
60
40
20
0
L
non-L
current density (pA/pF)
ctrl
nife
tox
Cd2+
***
b
-50
0
-90
command mV
Cd2+
apa
nife
tox
ctrl
100 pA
1 s
% of current
current density (pA/pF)
**
*
c
BAPTA
EGTA
ctrl
τslow
2.0
1.0
0
EGTA
BAPTA